Electrical and Mechanical Performance of Aluminum Alloys with Graphite Nanoparticles

A thesis presented to
the faculty of
the Russ College of Engineering and Technology of Ohio University

In partial fulfillment
of the requirements for the degree
Master of Science

Aditya K. Nittala
May 2019

This thesis titled

Electrical and Mechanical Performance of Aluminum Alloys with Graphite Nanoparticles

by

Aditya K. Nittala

has been approved for

the Department of Mechanical Engineering

and the Russ College of Engineering and Technology by

Keerti Kappagantula

Assistant Professor of Mechanical Engineering

Dennis Irwin

Dean, Russ College of Engineering and Technology

ABSTRACT

Nittala, Aditya K., M.S., May 2019, Mechanical Engineering

Electrical and Mechanical Performance of Aluminum Alloys with Graphite Nanoparticles

Director of Thesis: Keerti S. Kappagantula

Aluminum alloys with improved electrical and mechanical performance are a highly sought-after due to their potential use as energy efficient conductors in power transmission, electronics, and aerospace systems. In this thesis, a novel hot extrusion alloying (HEA) process was used to synthesize aluminum/graphite nano-alloys using commercially available AA1100 and graphite nanoparticles (GNP) as precursors to improve electrical properties. The effects of GNP content from 0 – 1 wt.%, on the electrical and mechanical properties were evaluated. Results showed that the addition of 0.25 wt.% GNPs to the Al substrate improved its electrical conductivity by 2.1%, current density by 7.9%, ultimate tensile strength by 6.1% and yield strength by 30.3% compared to the control sample with no GNP additives. Improvements in electrical conductivity and current density were observed for all Al/GNP formulation at 60 °C and 90 °C. Ductility of the Al/GNP nano-alloys decreased with increasing GNP content. The improvement in Al/GNP electrical performance is attributed to GNP exfoliation at the temperatures and shear stresses experienced during hot extrusion, leading to the formation of highly conductive graphene particles.

ACKNOWLEDGMENTS

Dr. Kappagantula, you have been a constant source of support, knowledge, and inspiration; introducing me to this subject, and guiding me through my time as a master’s student. I am grateful and consider myself very fortunate to have been given a chance to enter this field of research as a novice with the confidence that you had in me. Along with what I have accomplished as a student and researcher, your faith in me is what helped me find new academic interests, friends, and a home in Athens.

My gratitude towards Dr. Kraft, whose amazing depth and breadth of insight into material science has played a hugely significant role in me loving what I worked on during my program. I also would like to acknowledge his disdain for my cat t-shirts, which often spurred me to work harder to find more of them in clothing stores.

I would like to thank my committee members Dr. Jay Wilhelm and Dr. Jixin Chen, for their valuable input into this research.

I would like to thank Mr. Randy Mulford and Mr. Thomas Boyle for their help and assistance during the project. I’d also like to thank my colleagues in lab, who have become my friends; especially Jake, with whom I closely worked with for my research. I have found a family away from home in my friends and roommates here in Athens. Finally, my thanks to my family back home, who have given me nothing but unconditional love and support, always giving me the confidence to succeed and accomplish what I wanted to do, most importantly during my times of doubt.

TABLE OF CONTENTS

LIST OF TABLES

Page

LIST OF FIGURES

Page

CHAPTER 1: INTRODUCTION

Commercial grade aluminum (Al), with a purity of 99.99%, is extremely soft and malleable, having a yield strength of 10 MPa [1]. Pure Al (99.990%) has an electrical resistivity of 2.66 μΩ·cm and corresponding electrical conductivity of 37.6 MS/m, or 64.94% IACS (International Annealed Copper Standard) [2]. Al has been extensively used in commercial electrical power transmission applications, with 13% of Al produced globally being used in the energy sector. Along with its electrical properties, the use of Al in energy transfer and power transport applications stems from its low density (2700 kg/m^3), which is approximately 30% of that of copper.

Alloying Al is essential to bolster the mechanical properties of the metal for sustained use in power transfer applications. However, alloying typically decreases the electrical performance of pure Al [3], [4]. This is because the electrical conductivity of a metal is dependent on the electron mean free path. The presence of impurities in Al microstructure increases electron scattering, decreases electron mean free path and therefore, leads to a decrease in electrical performance [5]. 'Electrical conductor (EC) grade Al' refers to AA1350 which was the most used Al alloy in electrical applications up to the 1970s. However, it also has a large thermal expansion coefficient, creep failures, and galvanic corrosion issues when put in contact with copper connectors in electrical systems. Having been recommended for use in the National Electric Code (NEC) section 130.14 in 1987 [6], the use of AA8000 series alloys began gaining traction in wiring and power transmission applications, as it offered improved mechanical properties and thermal and chemical stability, compared to EC grade AA1350 alloy.

Addition of conductive nanocrystalline materials in Al matrices to enhance their bulk electrical properties became an active area of research in the last decade [7].

Recently, metals embedded with carbon based nanoscale additives such as carbon nanotubes (CNTs) and graphene have been the subject of intense research since significant enhancements in mechanical [8]–[11], thermal [12]–[14], and electrical properties [15]–[17] of the metal were reported. As shown in Figure 1, CNTs and graphene are carbon allotropes with the π conjugated electronic structure of sp^2 hybridized carbon atoms[18].

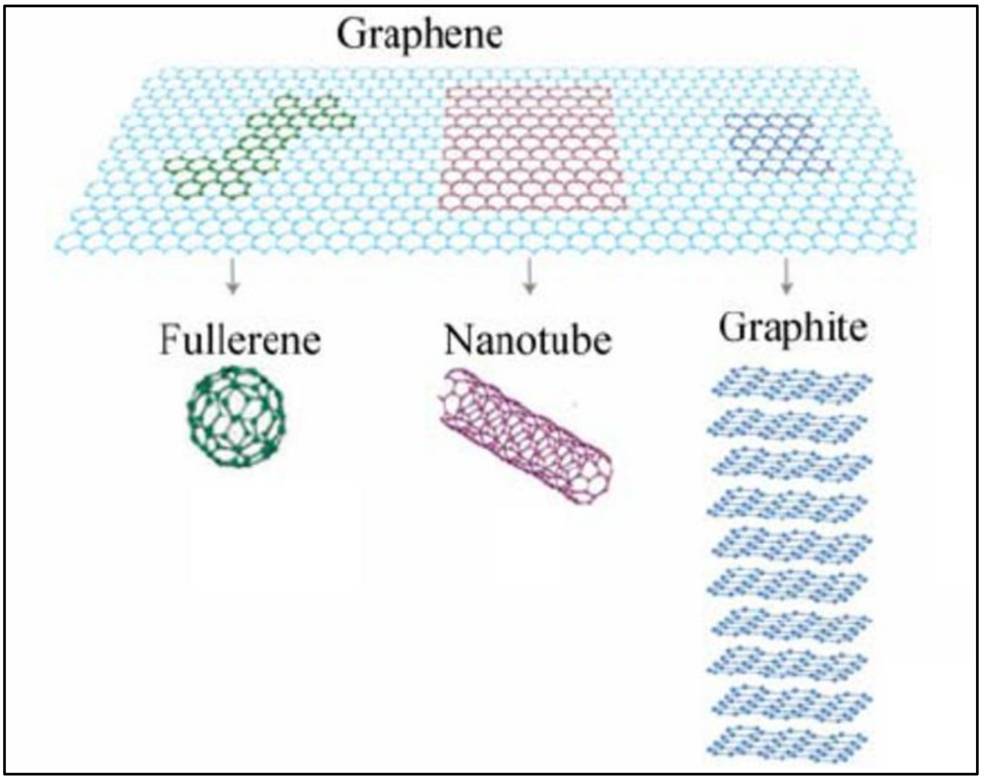

Figure 1. The allotropes of nanoscale carbon [19] .

More specifically, graphene is a two-dimensional array of carbon atoms arranged in a honeycomb structure; three of the four valence electrons of each carbon atoms form covalent bonds, while the remaining electron occupies the π orbital which is out-of-plane relative to the honeycomb/hexagonal array. The group of un-bonded electrons form a delocalized cloud, and serve as electrical charge carriers, as seen in Figure 2 [20]. This phenomenon, coupled with its low-defect 2D atomic lattice [21], results in unusually high thermal, mechanical and electrical properties [22]. Since its discovery in 2004 [21], graphene has found use in a wide range of applications ranging from transparent conductive media and flexible electronics [23], nanoelectromechanical systems [24], to composite filler material and heat removal systems. [25].

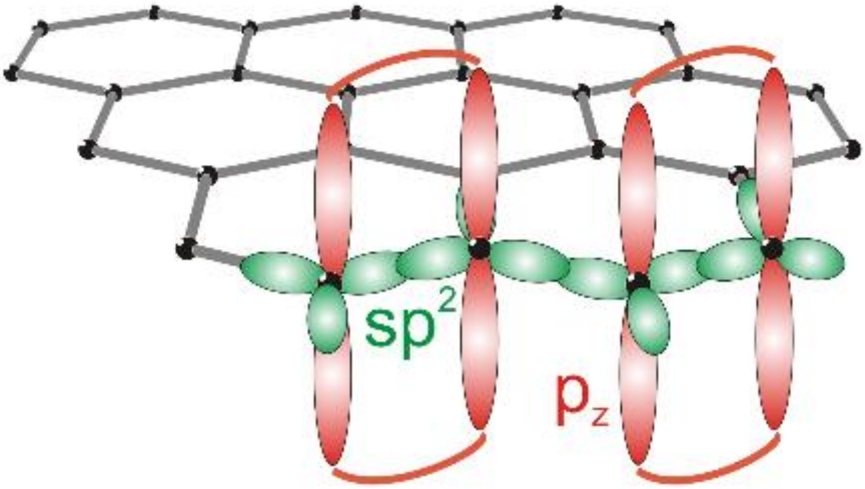

Figure 2. Schematic of graphene showing sp^2 hybridized carbon atoms forming the honeycomb array [26]. The unbonded p_z-orbital perpendicular to the plane of the array forms the π electron cloud.

Like CNTs, the appeal of graphene stems from superior intrinsic properties, such as ballistic electron conduction and high carrier mobility [21], [27], Young’s modulus of 1 TPa [28], high thermal conductivity of 3000-5000 W/ m·K [29], and high optical transparency of 97.7% [30]. The sturdy atomic structure and the planar two-surface nature of graphene sets an avenue for extensive interfacial chemistry when used in composites [31].

Graphene offers distinct advantages over CNTs when used as an electrical conductor or composite filler material. Graphene is a zero bandgap conductor, whereas CNTs display semiconductor/metallic conductor properties depending on their diameter (the bandgap of the electrons is inversely proportional to the diameter of the CNTs [32]), and their chirality [7]. The orientation of the atoms (i.e. the chirality of the CNT) determines its nature; CNTs demonstrate semi-conductor nature in the armchair configuration, and the zigzag configuration enables one-dimensional metal behavior [33], [34]. Due to the curved nature of the hexagonal unit cells of CNTs, the carbon atoms exhibit a quasi-sp^2 hybridized structure, whose electron conductance mechanisms are influenced by phonons, and becomes ballistic in nature at low temperatures [35]. Graphene, on the other end, is a planar sheet of sp^2 bonded carbon atoms. This structure can aid in more effective grain wrapping [36], and needs less control over directional orientation and chirality than CNTs to enhance electrical conductivity. This makes graphene a preferred additive for embedding into an Al matrix to improve its conductivity.

Manufacturing Al composites with graphene additives is typically riddled with persistent challenges such as achieving effective interfacial contact between the Al substrate and graphene, achieving homogeneity of graphene in the metal substrate, and ensuring that this second phase retains its topography and form in the composite without reacting with the metal to form undesirable intermetallic products, namely aluminum carbide. Reported techniques to make Al composites are powder metallurgy [9], [37]–[39], liquid metallurgy [17], [40]–[42], and spray deposition [43]; however, all of these processes, while successful in manufacturing Al/graphene composites with improved mechanical performance have thus far not been successful in improving the electrical performance of the resultant material. There is a critical need to develop an apt manufacturing approach that synthesizes graphene embedded Al substrates with minimal porosity, low oxide contamination, no intermetallic compound formation, and a homogeneous distribution of graphene in metal substrate.

Since the products manufactured are used in high-volume, the manufacturing process developed needs to be high-volume, easy-to-scale, and economically viable. Additionally, since the graphene embedded Al material may have to be post-processed depending on the type of electrical conductor component of interest, it has to demonstrate formability. This implies that it is desirable to manufacture Al alloys with second phase graphene or graphene-like additives in the microstructure that aid the charge transport efficiency as opposed to the traditionally envisaged Al/graphene metal matrix composites with low ductility.

Kappagantula *et al*. recently developed the hot-extrusion alloying (HEA) process to manufacture copper and Al based alloys with graphene and graphene-like additives in the material microstructure [44] to make industrially relevant bulk-size wire samples with minimal porosity, and homogeneous nanoparticle distribution. In this project, graphite nanoparticles (GNPs) comprising of <10 graphene layers were used to make Al nano-alloys. It was hypothesized the shear stresses developed during the alloy manufacturing process would delaminate the GNPs into monolayer or very few-layer graphene and embed them at the grain boundaries of the Al/GNP nano-alloy. This study explored the effects of GNP content on the electrical and mechanical properties of Al nano-alloys with embedded GNPs synthesized using the hot extrusion alloying process.

CHAPTER 2: OBJECTIVES

The primary goal of this project was to improve electrical performance of a 1000 series aluminum using GNP additives, thereby creating a unique nano-alloy. The effects of GNP concentration on electrical properties, as well as on mechanical properties were also assessed. To that end, the following objectives were identified.

2.1 Objective 1:

The first objective of this thesis was to improve electrical performance of aluminum using GNP additives and assess the effects of GNP content on the electrical properties of the Al/GNP nano-alloys synthesized.

To achieve this objective, Al/GNP nano-alloys with GNP content varying from 0 to 1 wt.% were synthesized using the HEA process. Electrical conductivity at room temperature and current density at 60 °C and 90 °C were determined for each Al/GNP composition as per ASTM B193.

2.2 Objective 2:

The second objective of this thesis was to assess the effects of GNP additive content on the mechanical properties of Al/GNP nano-alloys. The intent of this objective was to improve strength without adversely affecting ductility in the nano-alloy.

To achieve this objective, Al/GNP nano-alloys with GNP content varying from 0 to 1 wt.% were synthesized using the HEA process. The % elongation, yield strength, and ultimate tensile strength were determined for each Al/GNP composition as per ASTM B557M.

CHAPTER 3: LITERATURE REVIEW

Most published research on Al/graphene composites is focused on strength enhancement [9], [11], [45]–[50]. However, there are only few studies focused on manufacturing conductive Al/graphene composites and studying their electrical performance.

Powder metallurgy is the most reported processing method for making Al/graphene composites. Typically, graphene or reduced graphene oxide slurry is dispersed in solvents such as acetone [45], [47], isopropanol [11], ethanol [14], [51], [52] or deionized water [46], [53] and sonicated for homogenous dispersion of the additive flakes. The graphene dispersion is then ball milled with micron-sized Al or Al alloy powder, with control agents such as stearic acid [9], [11], [47], [50], [54] to prevent agglomeration of the graphene flakes. Post milling, the samples are sintered under pressure to consolidate the Al matrix and the additive at temperatures ranging from 300 °C – 600 °C to form Al/graphene composite. Mechanical property characterization in these studies reported a range of improvements compared to control samples, depending on the processing technique adopted. These are summarized as listed in Table 1.

Table 1. Compilation of reported values of mechanical properties of Al/graphene composites.

Author (s)	**Graphene content (wt.%)**	**% Increase in yield strength (YS)**	**% Increase in Ultimate Tensile Stress (UTS)**
Rashad *et al*. [45]	0.30	14.71	11.11
Yan *et al*. [52]	0.50	49.07	25.20
Shin *et al*. [11]	0.7 (vol. %)	71.80	-
Rashad *et al*. [51]	1.00	55.20	68.71
Tian *et al*. [47]	1.00	29.46	9.14
Li *et al*. [54]	1.00	34.90	-
Yolshina *et al*. [49]	2.00	16.02	51.58

Table 1 continued

Brown *et al.* [55]	3.00	30.00	2.73
Jain *et al.* [53]	6.00	-	57.80
Chyada *et al.* [56]	0.50	-	168.6
Lie *et al.* [39]	6 (vol. %)	-	110

Liquid metallurgy is another Al/graphene composite synthesizing process, involving the dispersion of reinforcements of the metal or alloy matrix in molten state, followed by casting. Composites are typically stir casted by generating a vortex which effectively disperses them [57], or by melt infiltration in which molten matrix metal or alloy is directed into a preform of the reinforcement material, and then allowed to solidify [58]. The process is carried out in an inert protective atmosphere, to eliminate oxidation of the metal surface at temperatures past the melting point [40], [58].

The primary advantages of liquid metallurgy based sample synthesis are the high production rate and the economic viability [59]. One of major problems is that this method utilizes the wettability of Al with the reinforcement material to ensure good interfacial contact in liquid phase; graphite is poorly soluble in molten Al, having a contact angle of 140° - 160° [7], made worse by the Al_2O_3 layer that forms readily on the surface on exposure to air. To decrease the contact angle and therefore, improve the wettability of molten Al with the reinforcement dispersion, materials like magnesium [57], copper [60], [61], nickel [62] or silicon carbide [63] were either coated on the reinforcement surface, or used as alloying constituents in the Al matrix. Yolshina *et al.* [49] synthesized graphene *in situ* using molten electrolytic halide mixtures in a 99.35% pure Al melt.

Another major problem associated incorporating graphene in Al matrix via liquid metallurgy is the susceptibility of Al to react with carbon at temperatures above 500°C, to form aluminum carbide (Al_4C_3) [36]. Given that liquid metallurgy processing usually has the molten Al maintained at temperatures above 700°C during synthesis, there are very strong possibilities of aluminum carbide formation in the melt. The presence of Al_4C_3 in Al/graphene composites is deleterious to their electrical properties; as it forms, it deforms the pristine sp^2 hybridized structure of graphene, which is essential to maintain its ballistic electron transport properties [9]. Al_4C_3 is electrically insulating Al and inhibits electronic interaction between Al and graphene. It also readily hydrolyzes, leading to accelerated corrosion of the Al surface [10]. Al_4C_3 formation is initiated typically at prismatic edges or exposed basal edges of graphene, which are created due to distortion or sheet fracture occurring under mechanical stress [3], at elevated temperatures.

A solid state processing method used to incorporate graphene in Al matrix while avoiding problems associated with liquid metallurgy is friction stir processing (FSP) [39], [64]. This method is a surface modifying technique, where a rotating tool stirs the surface of the metal substrate; the reinforcement is placed in this region in the form of a suspension in a groove or reservoir. Due to the localized softening induced by the heat of friction, the substrate plastically deforms, and the reinforcements are dispersed along the path of the rotating tool. Jeon *et al.* [64] reported a 15% increase in thermal conductivity, 50.5% increase in ductility, and a decrease of 12% in UTS of AA5052-H32 alloy reinforced with reduced graphene oxide (rGO). The rGO flakes were an average of 1 nm in thickness, and 1-3 µm in length. The authors attributed the rise in thermal conductivity to the reduction of GO into thermally conductivity rGO. The rGO was formed by the localized heating due to friction and plastic work during FSP [64].

Several problems are associated with Al/graphene composites fabricated using powder metallurgy techniques, such as nanoparticle additive agglomeration and porosity in microstructure. The intrinsic properties of synthesized composites are strongly influenced by the processing techniques. A steady decrease in density of the Al/graphene composites was demonstrated by Latief *et al*. with the increase of the wt.% of exfoliated graphene nanoplatelets due to the increased presence of agglomerated graphite [65]. Additionally, porosity in the composites is a prevalent issue which may be explained due to multiple factors. If metal particles are used as composite precursors, the presence of aluminum oxide (Al_2O_3) around the individual micron size particles inhibits effective substrate consistency [8], [66], along with preventing adhesion of the carbon nanostructure with the metal matrix, leading to significant porosity. Shrinkage during sintering, and trace quantities of graphene solvents or surfactants also contribute to porosity.

The formation of Al_4C_3 at the material interfaces is generally not desirable but is a prevalent issue in manufacturing Al/graphene composites using powder metallurgy techniques. Mechanical pressure on graphene during milling, along with defects on the plane due to thermal exfoliation of additive sheets lead to fraying of its edges [7]. This leads to the formation of chemically active sites, which trigger the reaction between Al and graphene, forming Al_4C_3 at the interface between Al and graphene. Al_4C_3 typically has a needle [37], [48] or platelet-like [67] morphology. Trace quantities of Al_4C_3 have been hypothesized to aid in interfacial bonding and effective load transfer between Al and carbon nanoparticles [8]. The formation of Al_4C_3 allows for localized stress contrast along the Al/graphene interface. This contributes to the anchoring effect of the reinforcement in the matrix, improving the mechanical characteristics of the Al composite [68]. However, large quantities of Al_4C_3 reduce the effectiveness of the embedded graphene, reducing them to areas of brittle reinforcements in the matrix [9].

There have been limited number of studies investigating the electrical performance of Al/carbon-based composites, summarized in Table 2.

Table 2. Compilation of reported values of electrical conductivity changes of Al/nano-carbon composites.

Author (s)	Additive	Additive concentration (wt.%)	% Increase in Electrical Conductivity
Brown *et al.* [55]	Activated carbon flakes	3	0.92
Xu *et al.* [16]	CNT	1	-30.6
Zameshin *et al.* [69]	C60	1-8%	-15.00
Tokutomi *et al.* [70]	CNT	0.1 (vol. %)	3.95
Chyada *et al.* [56]	Graphene	0.5	8.9

Xu *et al.* [16] evaluated the room temperature and cryogenic electrical conductivities of powder compacted Al/CNT composites by varying the CNT content. The composites were synthesized by compacting and hot pressing 99.5% pure Al powder of average of 74 µm (200 mesh) and CNT having an average diameter of 30 nm and lateral dimensions in a 1-3 µm (1, 4 and 10 wt.%) at 520°C and 25 MPa pressure for 30 minutes. At room temperature, the pure Al control sample's electrical conductivity was reported to be 29.41 MS/m. The 1 wt.% sample showed an electrical conductivity of 20.41 MS/m, which was a 30.6% decrease compared to the control sample. The 4 wt.% and 10 wt.% samples showed an electrical conductivity of 15.15 MS/m and 18.18 MS/m respectively, a decrease of 48.48% and 38.18% compared to the control sample. The authors attributed this decrease in electrical performance of the Al/CNT samples to the possible semiconductor nature of the CNTs, CNT agglomeration at the grain boundaries, and the formation of Al_4C_3 at the Al-CNT interface. Xu *et al.* also proposed that the decrease in electrical conductivity of Al/CNT composite may be due to improper consolidation of the CNT due to hand grinding, low loads applied during hot-pressing in which may have led to high porosity and poor interfacial bonding [36].

Zameshin *et al.* [69] studied the electrical and mechanical performance of composites fabricated using fullerene (C_{60}) powder and ultra-pure (99.999%) Al shavings. The samples were prepared by mixing Al shavings with the C_{60} particles with content varying between 1 – 8 wt.% in an argon atmosphere. The Al/C60 mixture was ball milled for 30 - 60 minutes after mixing, and then sintered at 250 °C – 280 °C for 15 – 20 minutes. The resulting billet was extruded into 3 mm diameter wire at 290 °C. The influence of cold pressing and annealing at 190 °C and 250 °C on the electrical conductivity of the 1 wt.% sample was determined. Zameshin *et al.* evaluated the mean crystallite size, electrical conductivity, and the hardness of the samples by varying the sintering and compaction parameters of the fabrication process. They also evaluated the mean crystallite size and electrical conductivity by varying the mass fraction of the C_{60} particles in the composite. The authors found that mean crystallized size of the grains decreased with increasing C_{60} content. A decreasing trend was also observed in the electrical conductivity values- a maximum value of 22.5 MS/m at 1 wt.%, compared to the control sample's electrical conductivity of 26.5 MS/m.

Tokutomi *et al.* [70] synthesized composite samples containing 99.9% pure Al with an average size of 50 µm, and multi-walled carbon nanotubes (MWCNTs) which had an average diameter of 65 nm, average length of 10 µm and an average of 70 carbon layers. The MWCNTs content in the composite was maintained constant at 0.1 vol.%. The composite samples were fabricated by initially ultrasonicating MWCNT and Al powder in ethanol, along with 2 ml of N-dimethylformamide. After the solvents were evaporated, the mixture was compacted at room temperature over a range of pressures ranging from 62 MPa to 748 MPa. The Al/MWCNT billets were subjected to sintering and hot extrusion at 500 °C with an extrusion ratio of 6.25. With increasing compressive stress, the control sample showed increasing electrical conductivity, with a peak of 61.77 IACS at 561 MPa. The electrical conductivity of the Al/MWCNT sample cold pressed at 561 MPa was 64.21 IACS, an increase of 4% compared to the control sample. The 0.2% offset YS, UTS, and the elongation of this sample during tensile testing were 45.9 MPa, 68.1 MPa, and 45.8% respectively, compared to the control sample's 0.2% offset YS of 40 MPa, UTS of 65 MPa, and elongation of 52%. The authors reported the presence of open ended CNTs embedded in the grain boundaries of the Al microstructure and attributed the improvement in the interfacial contact between the Al matrix and CNTs to increasing charge transfer across the interface. Similar results and electrical conductivity improvement mechanism were also previously reported by Gao *et al.* [71].

Chyada *et al.* [56] evaluated the effect of cold rolling and heat treatment on the electrical and mechanical properties of recycled 99.5% pure Al/graphene composites. The Al was obtained by melting electrical wire scrap and removing slag. The main impurities of recycled Al were silicon (0.11%) and iron (0.42%). The Al was reinforced with 0.5 wt.% graphene, prepared by pyrolyzing asphalt mixed with 30 wt.% ethanol. The authors employed a liquid metallurgy process, stir casting molten Al and dispersed graphene at 750 °C. The cast billet was wire-drawn in a 13-step process, to obtain 3.5 mm diameter wire from the initially cast 10 mm diameter rod. Prior to heat treatment, the pure Al wires were recorded to have an electrical conductivity of 33.8 MS/m (58.27 IACS) and UTS of 67 MPa. The Al-0.5 wt.% graphene sample showed an electrical conductivity of 33.3 MS/m (57.41 IACS) and UTS of 92 MPa, before heat treatment. The heat treatment regimen included holding the wire samples at 490 °C for 45 minutes, followed by quenching, 90% cold rolling, and artificial aging of the samples at 200 °C for 1 to 10 hours. The composite sample which was artificially aged for 1 hour showed the highest electrical conductivity of 36.8 MS/m (63.44 IACS), an improvement of 9% compared to the pure Al sample. This sample also had the highest UTS of 180 MPa, which was a 168% improvement over the control sample. With the variation of aging time, the electrical conductivity and the UTS showed similar trends- the sample aged for 1 hour showed the highest improvement. As the aging time increased up to 10 hours, the electrical conductivity and UTS both decreased and then stabilized at approximately 36.6 MS/m (63% IACS) and 148 MPa respectively.

There has been significant research in the field of Al/nanocarbon composites to improve the mechanical properties of Al, for its application in the construction, automotive and aerospace industries. Attempts were also made to characterize the thermal properties [64], [72], corrosion resistance [73], tribological properties [74], [75]. As summarized in this section, there has been limited research investigating the methods to improve the electrical properties of Al by synthesizing Al composites with nanocarbon additives. Some of the important challenges in this area of research are the reduction of Al_4C_3 formation, understanding the nature of the interfacial electron transfer between the Al matrix and carbon reinforcements, and developing a process to synthesize industrial scale quantities of Al/graphene composites with improved electrical properties.

CHAPTER 4: EXPERIMENTAL SECTION

4.1 Materials

In this study, AA1100was used as the base material. The composition of the AA1100 material is shown in Table 3. GNP additives with an average particle thickness of 3 nm and lateral size of 2 - 8 µm were obtained. Isopropyl alcohol with a purity grade of 99.5% and commercial grade Al foil with a thickness of 13 µm were obtained.

Table 3. Chemical composition of AA1100 substrate used in this study [76].

Element	Silicon	Iron	Copper	Manganese	Zinc	Al
Content (wt.%)	< 0.95 (together)		0.05 – 0.20	0.05 max.	0.10 max.	99.00 min.

4.2 Sample Preparation Method

The Al/GNP nano-alloy was synthesized using the HEA process in this work. Initially, requisite quantities of GNPs were suspended in 60 mL isopropanol to synthesize a GNP ink which was sonicated using a Qsonica500 ultrasound sonicator for 30 mins. Subsequently, the GNP inks with varying GNP concentrations were deposited onto AA1100 profiles. Each GNP ink droplet was estimated to have an average size/average volume of 0.01 ml. The profiles were placed in a fume hood and heated at 100 – 150°C for about 20 mins to evaporate isopropanol completely leaving behind the GNPs alone. Subsequently, the GNP coated metal profiles were consolidated and wrapped in commercial grade Al foil to form a cylindrical billet pre-form with a length of 50 – 60 mm and a diameter of 15.6 mm. The billet pre-form was cold pressed at 560 MPa for approximately 10 mins. A 250 kN MTS extrusion apparatus developed by Kraft *et al.* [77] was used to manufacture the Al/GNP nano-alloy samples from the billet pre-forms (Figure 3). The extrusion apparatus uses a computer controlled 250 kN servo-hydraulic MTS® load frame. Sample heating is achieved with cartridge heaters placed in the container and die holder. Thermocouples in the apparatus provide feedback to the PID controllers and are used for temperature date acquisition. A thermocouple placed in the die holder is the most accurate indicator of the die temperature during extrusion, since it is placed closest to the deformation zone during extrusion.

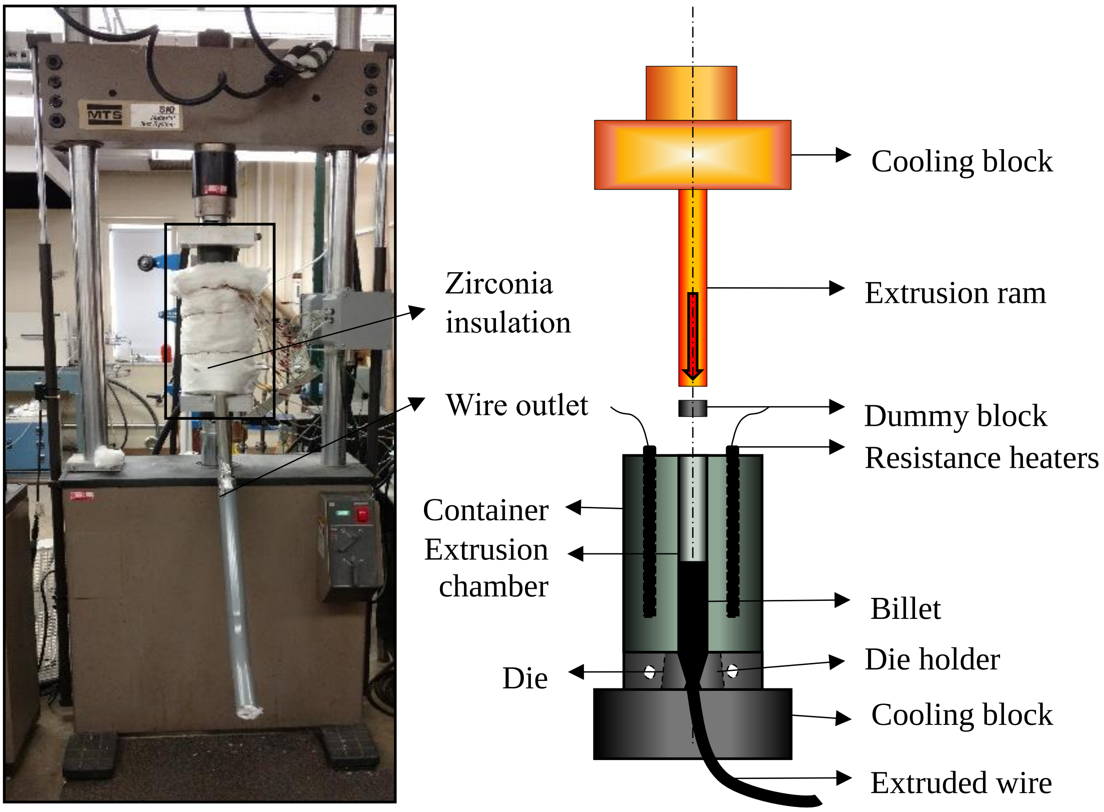

Figure 3. (left) MTS extrusion machine used for fabricating the Al/GNP nano-alloy wire; (right) schematic of extrusion apparatus.

The Al/GNP billet pre-form was heated initially to 500°C for 40 mins and then hot-pressed at the same temperature with pressures in the range of 11 MPa – 45 MPa for 20 mins. Using a conical die with semi die angle of 45° and an extrusion ratio of about 60, the billets were extruded to a diameter of ~2 mm. The velocity of the ram was maintained at 0.05 mm/s, to achieve approximately isothermal conditions during extrusion and cool the wire in the nitrogen-filled outlet tube. The ram speed, displacement and force were recorded at a sampling rate of 10 Hz, and the temperatures during billet heating and extrusion were recorded at a sampling rate of 1 Hz. Nano-alloy samples were manufactured to have GNP content ranging from 0 – 1 wt.%, namely 0 wt.%, 0.25 wt.%, 0.5 wt.%, and 1 wt.%.

4.3 Characterization of Sample

4.3.1 Sample Dimensions

The length of the nano-alloy samples was measured using a Kobalt 293883 digital calipers with an accuracy of 10 µm. The wire diameters were measured with a Keyence LS-7601 optical micrometer, shown in Figure 4.

Figure 4. Keyence LS-7601 Optical Micrometer.

The wires were placed between the transmitter-receiver setup of the optical micrometer perpendicular to its orientation and were moved along its length to record 10 different readings of its cross-sectional diameter along the length. The average of these readings was then calculated and presented as wire diameter *d*.

4.3.2 Electrical Conductivity Measurement

Electrical conductivity of the Al/GNP nano-alloy samples was determined by measuring the resistivity using the four-point probe method as per ASTM B193 [78].

Voltage drop was measured using a Keithley 2182A Nanovoltmeter (accuracy 0.002% ± 1 mV) and Keithley 2260B-30-72 Bench Power Supply (accuracy 0.1% ± 20 mV, 0.1% ±70 mA) was used to supply current through the sample. The wire sample is clamped under tension across a custom-built base. Two pairs of electrical leads were connected in parallel across the wire sample as shown in Figure 5. One pair of leads supplied the test current to the wire sample, and the other pair of leads was connected to the nanovoltmeter, whose readings were used to calculate sample resistance.

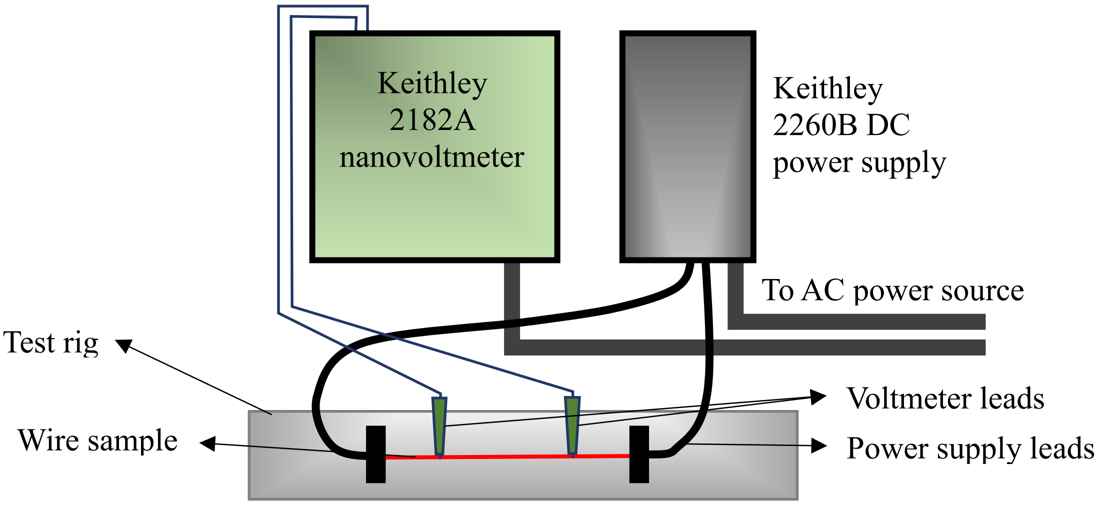

Figure 5. Four-wire method for measuring electrical conductivity.

As per Ohm's law, the resistance *R* of a conductor is given by

$$R = \frac{V}{I} \qquad \text{Equation (1)}$$

where *V* is the DC voltage measured across the sample length *l* of the wire, and *I* is the input current from the power supply. Accordingly, electrical conductivity (σ) of the samples was measured using Equation (2).

$$\sigma = \frac{4l}{R\pi d^2} \qquad \text{Equation (2)}$$

4.3.3 Current Density Testing

In this test as shown in Figure 6, the wire samples were supplied with DC current from a Keithley 2260-30-72 power supply via Joule heating.

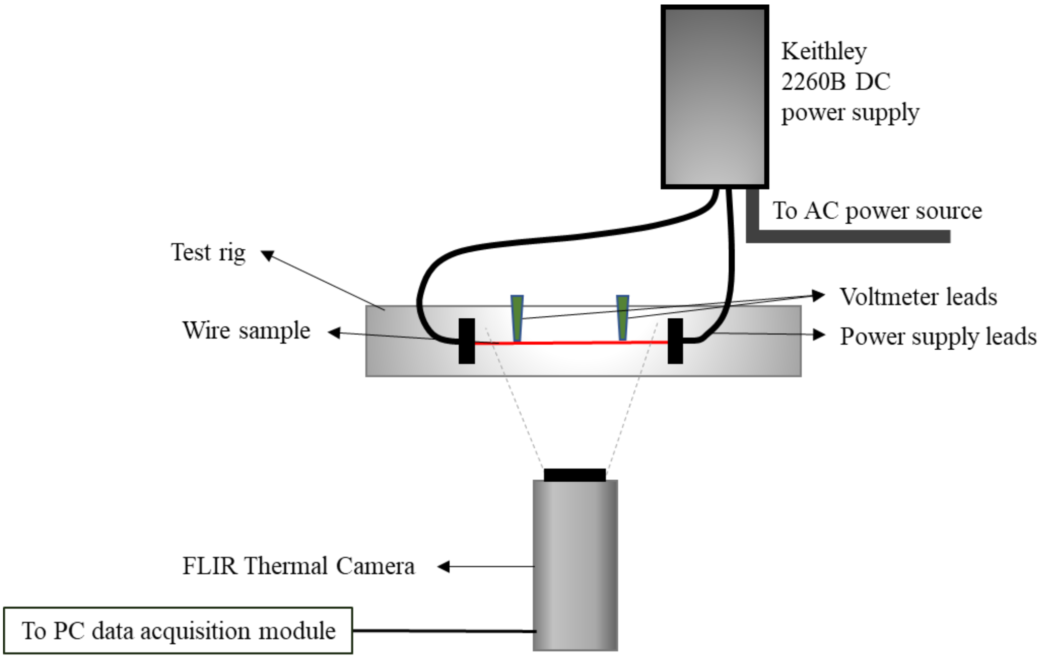

Figure 6. Schematic of current density test for measuring current density of wires.

An FLIR A325SC thermal camera with an accuracy of ±2 °C, calibrated using an IR-2013/301 blackbody, was used to measure the real time non-contact temperature of the sample wire at each current level. Prior to current density measurement, the wires were coated with a layer of black graphite paint to render the emissivity of the surface to be ~0.99. The temperature of the sample was monitored until the rate of change of temperature was determined to be less than 0.5 °C/s for at least 5 minutes after which steady state was assumed to have been achieved. The temperature of the wire as measured by the IR camera at each particular current was recorded. This procedure was adopted for currents ranging from 20 – 45 A (in multiples of 5 A). The steady state temperatures were determined as a function of current. Regression analysis was performed to find the relationship between the current and wire temperature for each sample. This curve-fit equation was then used to calculate the current flowing through the wire samples at 60 °C and 90 °C, and consequently, its current density as per Equation (3).

$$J = \frac{4I_{\mathrm{T}}}{\pi d^2} \qquad \text{Equation (3)}$$

where I_{T} is the current passing through a wire at a given temperature T.

4.3.4 Tensile Testing

The stress-strain behavior of the wire samples was obtained during tensile testing as per ASTM B557M [79] using an Instron 5567 Material Testing Frame. The electromechanical frames apply a tensile load (monitored by a load transducer) to the wire specimen via the moving crosshead (Figure 7). The testing parameters were set with the Bluehill Instron software that is the interface to the machine.

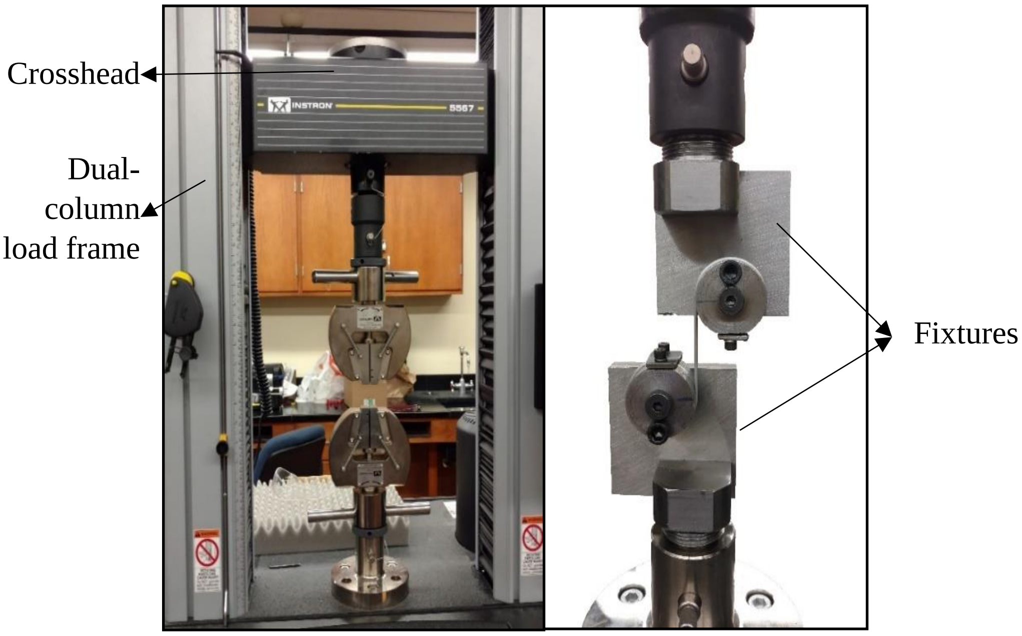

Figure 7. Instron 5567 material testing machine (left); tensile testing of Al/GNP nano-alloy wire with custom made fixtures (right).

The samples were attached to custom-made fixtures designed to accommodate shorter 12 AWG samples. Samples were pulled at a constant velocity, to provide an initial strain rate of 0.01 s^{-1}. Force and crosshead displacement data were recorded, and from these data the stress-strain diagrams were generated. The 0.2% yield stress was determined by establishing the linear elastic region of the curve and applying a 0.002 strain offset. The ultimate tensile strength of the wire samples was determined by dividing the maximum force by the initial cross-sectional area.

4.4 Uncertainty analysis

Uncertainty analyses were performed to characterize the performance capabilities of the testing configurations.

4.4.1 Electrical Conductivity Test Uncertainty

Electrical conductivity of the wire sample was given by

$$\sigma = \frac{4LI}{\pi V d^2} \qquad \text{Equation (4)}$$

The measured variables were:

- Current I
- Voltage V
- Wire diameter d
- Gauge length l

The root sum square uncertainty of conductivity U_σ is given by Equation (5):

$$U_\sigma = \sqrt{\left(\frac{\partial\sigma}{\partial I}U_I\right)^2 + \left(\frac{\partial\sigma}{\partial V}U_V\right)^2 + \left(\frac{\partial\sigma}{\partial d}U_d\right)^2 + \left(\frac{\partial\sigma}{\partial l}U_l\right)^2} \qquad \text{Equation (5)}$$

Table 4. Uncertainty analysis terms for electrical conductivity.

Parameter	**Description**	**Value**	**Source**
U_I	Uncertainty in current measurement (A).	$0.0001I$	[80]

Table 4 Continued

Parameter	Description	Value	Source
U_V	Uncertainty in voltage measurement (V).	$\frac{(60V + 0.04)}{10^6}$	[81]
U_d	Uncertainty in measurement of cross-sectional diameter (m).	3 x 10^{-6}	[82]
U_l	Uncertainty in measurement of gauge length of sample (m).	1 x 10^{-5}	-

4.4.2 Current Density Test Uncertainty

Current density was calculated by

$$J = \frac{4I_{\mathrm{T}}}{\pi d^2} \quad \text{Equation (6)}$$

The measured variables were:

- Voltage V
- Wire diameter d
- Temperature T

The root sum square uncertainty of current density U_J is given by:

$$U_J = \sqrt{\left(\frac{\partial\rho}{\partial V}U_V\right)^2 + \left(\frac{\partial\rho}{\partial D}U_D\right)^2 + \left(\frac{\partial\rho}{\partial T}U_T\right)^2} \quad \text{Equation (7)}$$

Table 5. Uncertainty analysis terms for current density calculation.

Parameter	Description	Value	Source
U_I	Uncertainty in current measurement (A).	$0.0001I$	[80]

Table 5 Continued

U_d	Uncertainty in measurement of cross-sectional diameter (m).	3 x 10^{-6}	[82]

4.4.3 Tensile Test Uncertainty

The tensile stress recorded at any point before fracture of the samples is given by

$$\sigma = \frac{4F}{\pi d^2} \qquad \text{Equation (8)}$$

The root sum square uncertainty of the tensile stress σ is given by:

$$U_E = \sqrt{\left(\frac{\partial \sigma}{\partial F} U_F\right)^2 + \left(\frac{\partial \sigma}{\partial d} U_d\right)^2} \qquad \text{Equation (9)}$$

Table 6. Uncertainty analysis terms for tensile testing.

Parameter	**Description**	**Value**	**Source**
U_F	Uncertainty in force measurement (N).	0.005	[83]
U_d	Uncertainty in measurement of cross-sectional diameter (m).	3 x 10^{-6}	[82]
U_l	Uncertainty in measurement of gauge length of sample (m).	0.0007	[84]

CHAPTER 5: RESULTS AND DISCUSSION

5.1.1 Objective 1

The first objective of this thesis involved assessing the effects of GNP additive content on the electrical performance of Al/GNP nano-alloys. To achieve this objective, Al/GNP nano-alloys with GNP content varying from 0 to 1 wt.% were synthesized using the HEA process. Electrical conductivity at room temperature (and up to 90°C) and current density at 60°C and 90°C were determined for each Al/GNP composition as per ASTM B193.

5.1.2 Results

The Al/GNP nano-alloy wire samples were tested for electrical conductivity as per ASTM standard B193 and the results are shown in Figure 8. Three replicates of nano-alloy wires at GNP concentration of 0 – 1 wt.% were made to ensure measurement repeatability. The electrical conductivity was determined based on 6 tests performed across 140 mm length per wire sample replicas. The calculated uncertainty for the measurement of electrical conductivity was 0.1 MS/m (0.18% IACS).

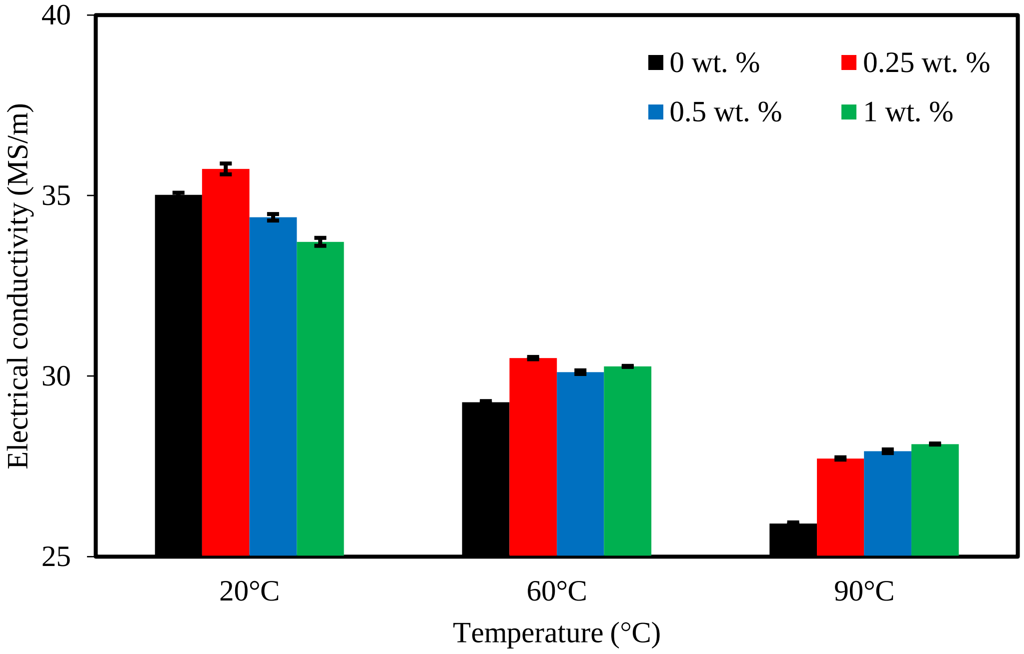

Figure 8. Electrical conductivity of Al/GNP nano-alloys with varying GNP content at 20 °C, 60 °C and 90 °C. The error bars signify the sample standard deviation.

The control sample with no GNP additives demonstrated an electrical conductivity of 35.0 MS/m, 29.3 MS/m, and 25.9 MS/m at 20 °C, 60 °C and 90 °C respectively, similar to the properties available for AA1100 in literature [4], [78]. The highest electrical conductivity of 35.7 MS/m at 20 °C was observed in the 0.25 wt.% Al/GNP sample, which was an increase of 2.1%, compared to the control sample with no GNP additives. A decrease in electrical conductivity at room temperature was observed when the GNP concentration was increased over 0.25 wt.%. The Al/GNP sample with 0.50 wt.% showed an electrical conductivity of 34.4 MS/m. Al/GNP with 1.0 wt.% GNP showed the lowest electrical conductivity of 33.7 MS/m, with a decrease of 3.7% compared to control sample.

The trends in electrical conductivity changed at higher test temperatures. At 60 °C, all the nano-alloys demonstrated improved electrical conductivity compared to the control sample with an electrical conductivity of 29.3 MS/m. The 0.25 wt.% sample once again demonstrated the highest electrical conductivity of 30.5 MS/m or an increase of 4.1% over the control sample. The 0.50 wt.% sample had an electrical conductivity of 30.1 MS/m, which is an increase of 2.8%, and the 1 wt.% sample had an electrical conductivity of 30.3 MS/m, an increase of 3.4%.

At 90 °C, the control sample had an electrical conductivity of 25.9 MS/m. The 0.25 wt.% sample showed an electrical conductivity of 27.7 MS/m or an increase of 6.9% compared to the control sample. The 0.50 wt.% sample had an electrical conductivity of 27.9 MS/m, an increase of 7.7%, and the 1 wt.% sample had the highest electrical conductivity of 28.1 MS/m, an increase of 8.5%.

Current density of the Al/GNP nano-alloy wires was measured at 20 °C, 60 °C and 90 °C. Five measurements at each current value were recorded during sample testing. The current density data are shown in Figure 9. The uncertainty in the current density measurements had a maximum value of 0.3 A/mm^2.

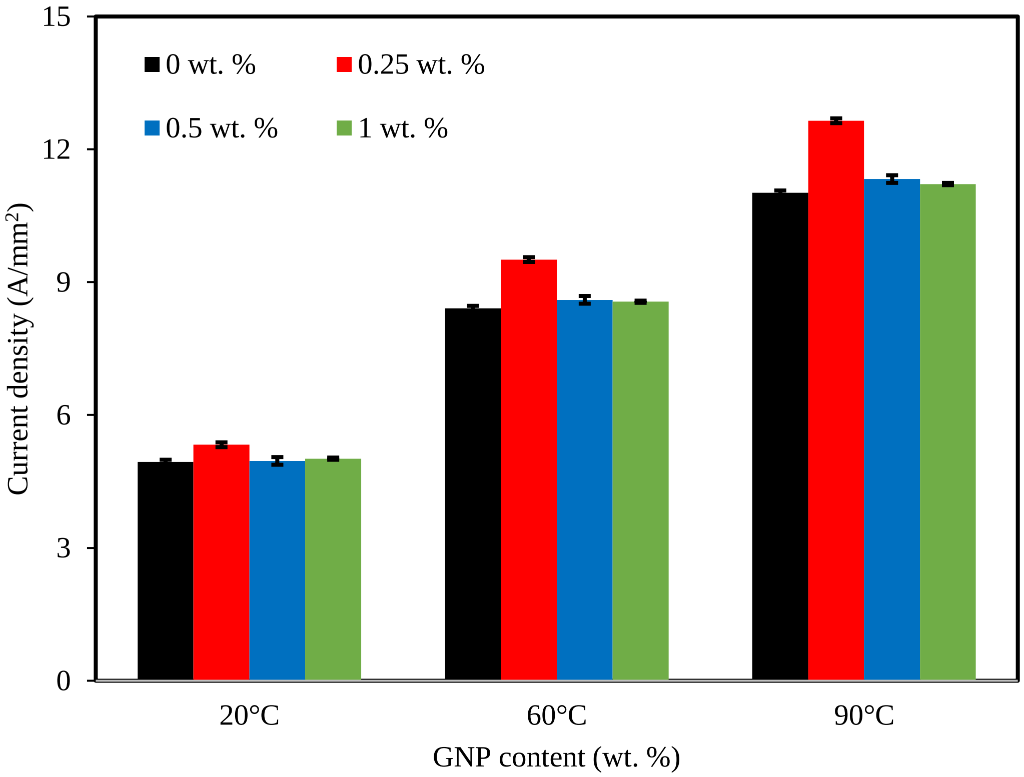

Figure 9. Current density of Al/GNP nano-alloy wires at 20 °C, 60 °C and 90 °C. The error bars signify the sample standard deviation.

The current density of the control samples was measured to be 4.9 A/mm^2, 8.4 A/mm^2 and 11.0 A/mm^2 at 20 °C, 60 °C and 90 °C, respectively. Interestingly, all the Al/GNP nano-alloy samples showed an improvement in current density compared to the control sample at all the temperatures at which the property was tested. The current density trend at each temperature was similar. The samples with no GNP additives showed the least current density. Addition of GNPs increased the current density to a maximum at a concentration of 0.25 wt.% GNP, after which it decreased for samples with 0.5 wt.% GNP and almost plateaued at 1 wt.% GNP samples. The Al/GNP nano-alloy sample with 0.25 wt.% GNP demonstrated the largest improvement in current density on the addition of GNP additives compared to the control sample wires with no GNP additives. It showed a current density of 5.3 A/mm^2 at 20 °C, 9.5 A/mm^2 at 60 °C, and 12.7 A/mm^2 at 90 °C respectively corresponding to an improvement of 7.9%, 13.1%, and 14.8% at respective temperatures with respect to the control sample.

Examining the electrical performance of the Al/GNP nano-alloys in the present study, it is evident that the addition of GNP elicits a uniquely significant improvement in the electrical conductivity and current density of the nano-alloy. The increase in electrical conductivity of Al/GNP with 0.25 wt.% GNP content may be somewhat counterintuitive since the presence of carbon in the Al matrix typically leads to a decrease in the electrical conductivity, as seen consistently in the literature [16], [69], [85]. Past studies showed that alloying Al with additives of limited solubility results in decreased grain size [39], [86], [87] and increased grain boundary density as well as increased material interfaces in the microstructure [88]–[90]. Mahmudi [88] attributed this phenomenon to the pinning of grain boundaries during recrystallization by intermetallic particles. While the microstructure of the Al/GNP nano-alloys manufactured in this study was not fully assessed, it is asserted that the addition of GNPs via the HEA process increases interfaces (i.e., Al-GNP) and most likely reduces grain size. The formation of Al_4C_3 is also possible under certain conditions. Both of these factors can lead to increased electron scattering in the microstructure and therefore, decreased electrical conductivity. Regardless, the results observed in this study are indicative of the presence of a significant amount of conductive additives in the Al matrix, actively participating in the electron transport processes. In fact, this is a plausible explanation for the enhanced electrical conductivity of the nano-alloy despite increased electron scattering at Al/carbon interfaces. However, GNPs alone cannot justify the improvement in nano-alloy conductivity since their electrical performance is much lower than that of Al matrix. The improved Al/GNP electrical performance may be explained by the presence of a sufficient number of graphene-like flakes in the Al matrix actively participating in the electron transport process. Electron mobility in graphene is orders of magnitude higher than that of Al, with graphene being reported to have mobilities in the range of 0.3 $m^2/V{\cdot}s$ - 2.7 $m^2/V{\cdot}s$ when compared to Al's measured value of 0.0013 $m^2/V{\cdot}s$ [91]. Therefore, if the Al/GNP microstructure contains a large number of single- or few-layer graphene particles, electrons can enter and exit them and move with high mobility and minimal scattering. Improved electrical performance of the bulk material is further explained by the development of a favorable interface between the Al and graphene that is conducive to electron exchange. The presence of graphene-like additives in the metal microstructure promotes the ballistic electron transport along their length [92], providing alternate pathways for charge transfer in the Al matrix while subjected to an electric potential. However, if graphene's presence alone in the microstructure can explain the uniquely improved electrical performance of the

Al/GNP nano-alloys, it is essential to explore its source in the nano-alloy. It is possible that the GNPs exfoliate into single- or few-layer graphene due to shear-stresses experienced by them in the deformation zone during the HEA process. The probability of GNPs exfoliating into graphene can be determined by examining the stress state in the deformation zone of the hot-extrusion stage in the HEA process. The GNPs can exfoliate if the shear flow stress in the deformation zone is greater than that needed to overcome the van der Waals bonds between graphene layers.

The flow stress (σ_f) exerted on the GNPs during deformation can be predicted as a function of the Zener-Hollomon parameter *Z* [93] as shown in Equation (10):

$$\sigma_f = \frac{1}{\alpha}\left(\ln\left(\frac{Z}{A}\right)^{1/n} + \sqrt{\left(\frac{Z}{A}\right)^{2/n} + 1}\right) \qquad \text{Equation (10)}$$

where α is the semi die angle of die used during extrusion, *A* is the pre-exponential factor, experimentally determined in the Arrhenius rate equation, and *Z* is the Zener-Hollomon parameter, given by Equation (11) below:

$$Z = \dot{\varepsilon}\exp\left(\frac{Q}{RT}\right) \qquad \text{Equation (11)}$$

In Equation (11), *Q* is the activation energy, which can be described as the energy barrier to initiate deformation or metal flow [94], *R* is the universal gas constant, *T* is the extrusion temperature, and $\dot{\varepsilon}$ is the strain rate given by Equation (12) as shown below [95]:

$$\dot{\varepsilon} = \left(\frac{6V\ln r}{D}\right)\tan\alpha \qquad \text{Equation (12)}$$

where *V* is the extrusion velocity, *r* is the extrusion ratio and *D* is the billet diameter.

Finally, the shear flow stress σ_f' experienced by the GNPs in the deformation zone during the HEA processing was determined by the von Mises criterion in Equation (13):

$$\sigma_f' = \frac{\sigma_f}{\sqrt{3}} \qquad \text{Equation (13)}$$

The HEA process and material parameters are listed in Table 7. The material parameters *Q*, *A*, and *n* for AA100 were determined empirically by curve fitting data derived from the literature [96].

Table 7. Values of parameters to calculate flow stress during extrusion.

Parameter/constants	**Notations**	**Values**
Ram speed (mm/s)	V	0.051
Die Entry temp (K)	T	773
Extrusion ratio	r	60
Billet diameter (mm)	D	15.88
Semi die angle (radians)	α	0.79
Activation energy (kJ/mol) [96]	Q	175.3
Universal Gas Constant (kJ/mol·K)	R	8.31
Pre-exponential factor [96]	A	1.91×10^{7}
Zener-Hollomon Constant	Z	1.93×10^{11}

The shear flow stress which was experienced by the GNPs was estimated to be about 28 MPa. In a recent study, Tran *et al.* [97] simulated the shear stresses developed during the shear-induced exfoliation of graphite flakes in a rotating fluid. By rotating the fluid in a Taylor–Couette flow reactor made of two rotating co-axial cylinders at 1000 rpm, the graphite flakes in the fluid were subjected to estimated shear stresses of 8 Pa. These shear stresses were found to be effective in exfoliating the graphitic flakes into few-layer graphene (FLG), which was characterized by Raman spectroscopy and X-ray photoelectron spectroscopy. The flow stress experienced by the GNPs in the deformation zone during the HEA process may be orders of magnitudes larger than the shear stresses required to overcome the van der Waals' forces between the sp^2 carbon layers in the GNP flakes in order to exfoliate them to form single- or few-layer graphene. Thus it is reasonable to assert that the HEA process exfoliates the GNPs into single- or few-layer graphene, which are then favorably distributed in the Al matrix during the Al/GNP nano-alloy synthesis.

Based on the electrical performance results of Al/GNP, it is also reasonable to deduce that there is minimal Al_4C_3 formation during the processing of the Al/GNP alloy. Any Al_4C_3 would presumably exist predominantly at the Al-graphene interface and disrupt electron transport from Al to graphene, and this would decrease the electrical conductivity and current density of the material. The fact that the addition of GNPs to Al lead to an improvement in the alloy's electrical performance implies that there was very little to no intermetallic compounds formed. For the exfoliated GNP to not adversely affect the electrical conductivity of the Al/GNP nano-alloy, it would have to be embedded along the grain boundaries, as the presence of GNP in interstitial positions within the Al grains would lead to electron scattering due to localized strain fields [98], [99]. This decrease in electrical conductivity is not observed in the 0.25 wt.% Al/GNP sample, which would imply the presence of GNP mainly along the grain boundaries of Al matrix.

It is noteworthy that the electrical conductivity of the Al/GNP nano-alloy decreases as a function of temperature. This behavior is similar to that of that the Al control sample. In metals like Al, this trend in electrical conductivity is attributed to an increase in electron scattering because of increased phonon density as temperature increases. This is caused due to increased degradation of the lattice symmetry in the metal grains due to increased thermal vibrations [100]. Additionally, charge carrier mobility also decreases in metals with increase in temperature [101]. However, from Figure 8, it can be seen that the decrease in the electrical conductivity of Al/GNP nano-alloys with respect to temperature was lower than that of the control sample with no GNPs. The reason behind this unique behavior of the Al/GNP nano-alloys may lie with the response of the single- or few-layer graphene flakes exfoliated from the GNPs during the alloy synthesis. Contrary to metal behavior, charge carrier mobility and electrical conductivity of graphene has been shown to increase with the increase in temperature. Fang *et al.* [91] examined the electrical behavior of single layer graphene, few layer graphene and graphene nanosheets at high temperature and observed that while the electrical conductivity decreased with increasing number of graphene layers, the increase in temperature of graphene improved the electrical conductivity and charge carrier mobility. The authors attributed this behavior to the negligible effect of temperature on the Fermi velocity of electrons in graphene, as the electron cloud was theorized to have minimal collisions with the graphene lattice. It was concluded by the authors that the scattering occurs more between electron-electron interactions than electron-phonon interactions, of which the latter is the main contributor to the decrease in conductivity due to increased temperature. The improvement in electrical conductivity of the Al/GNP nano-alloys at higher temperatures may therefore be due to the presence of single- or few-layer graphene flakes in the Al matrix with higher charge carrier mobility at higher temperatures leading to increased electrical performance compared to samples with no graphene-like structures. In fact, the electrical conductivity trends of the Al/GNP at higher temperatures seen in this study demonstrate important phenomena. GNPs most likely exfoliate into graphene flakes in the Al matrix, otherwise the electrical conductivity of the nano-alloys would decrease with temperature at a higher rate than that of the control sample with no GNPs. Furthermore, the graphene flakes actively participate in charge carrier transport in the alloy microstructure which is the reason why their behavior dominates the electrical performance of the Al/GNP nano-alloys at higher temperature, thereby the decreasing the rate of decrease in electrical conductivity with temperature.

Figure 8 also indicates that there might be a limit to the extent to which GNPs, and the graphene flakes derived from this approach may improve the electrical performance of the Al substrate. An increase in GNP content above 0.25% did not increase the electrical conductivity. In fact, it had the opposite effect by decreasing this property. The decrease in electrical conductivity in samples with 0.5 wt.% GNP and 1 wt.% GNP may be due to an increase of graphene flakes, whose agglomeration was not overcome by the HEA process conditions. This would reduce the conductivity of the bulk material. It is interesting to note that such agglomerations were evident on the surface of the nano-alloy samples with 0.5 wt.% and 1.0 wt.% GNP, as shown in Figure 10.

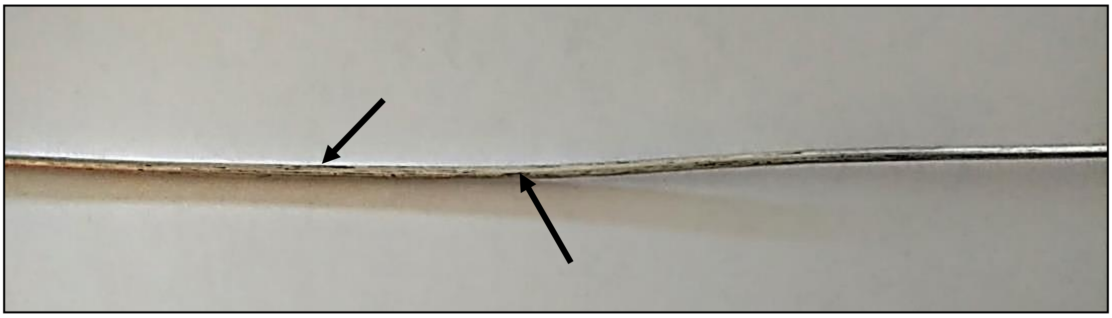

Figure 10. Agglomerations observed on the surface of the 1 wt.% Al/GNP sample.

The current density of individual samples during testing was found to behave in trends opposite to those observed in high temperature electrical conductivity whereby the current density increased with temperature. This is because of the method of testing involved in evaluating the high temperature electrical performance of the Al/GNP nano-alloys. While keeping the ambient temperature around the wire in the range of 19.5 °C – 20.5 °C, the sample length of wire was subjected to increasingly larger amounts of current, to cause a temperature increase in the wire via Joule heating. The power dissipated in the form of heat in the Al/GNP nano-alloy wire is given in Equation (14):

$$P \propto I^2 R \qquad \text{Equation (14)}$$

Where P is the power dissipated by Joule/ohmic heating, I is the current flowing through the Al/GNP wire sample, and R is the resistance of the Al/GNP wire sample. To produce a higher wire temperature, larger amounts of current were applied. Therefore, the amount of current per unit cross sectional area of the wires measured at elevated temperature (60 °C and 90 °C) were higher than that measured at room temperature.

The 0.25 wt.% sample measured a maximum current density of 5.3 A/mm^2, 9.5 A/mm^2, and 12.7 A/mm^2 at 20 °C, 60 °C and 90 °C respectively. This behavior was consistent with electrical conductivity performance of the Al/GNP nano-alloy wires. The 0.25 wt.% Al/GNP sample had the lowest electrical resistivity, and thus it is reasonable that a greater amount of current was required to raise the wire temperature to 60 °C and 90 °C, when compared to the control sample.

5.2.1 Objective 2

The second objective of this thesis involved studying the effects of GNP additive content on the mechanical properties of Al/GNP nano-alloys for GNP content varying from 0 to 1 wt.%. The elongation, yield strength, and tensile strength were determined for each Al/GNP composition as per ASTM B557M.

5.2.2 Results

To address objective 2, Al/GNP samples were synthesized with GNP content varying from 0 to 1 wt.%. Three replicates of each nano-alloy composition were tested to ensure measurement repeatability. The synthesized nano-alloy wires were subjected to tensile testing as detailed in Section 4.3.4 to evaluate their deformation behavior under tensile conditions as well as their 0.2% offset yield strength, tensile strength, and total elongation. Figure 11 presents the tensile characteristics of the synthesized of Al/GNP nano-alloys samples.

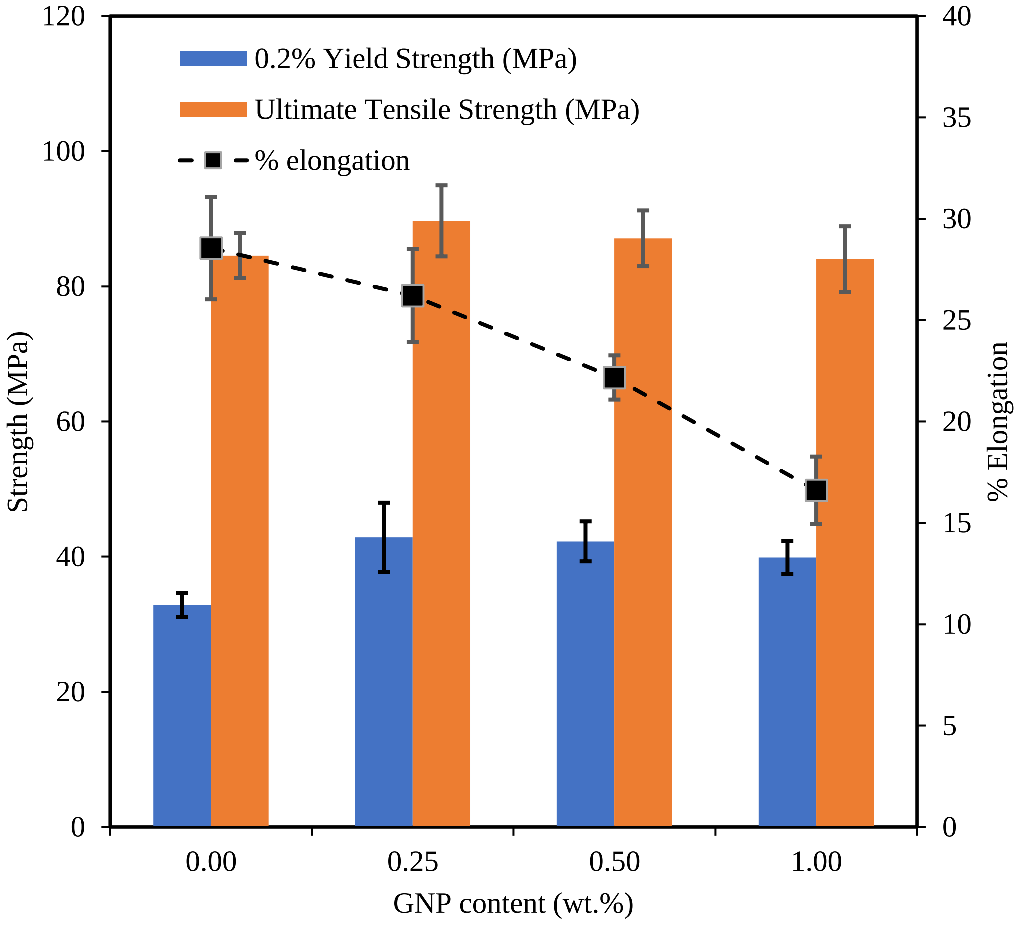

Figure 11. Tensile characteristics of Al/GNP nano-alloy wires. The error bars signify the sample standard deviation.

As observed in Figure 11, the control sample with no GNPs comprising of AA1100 alone demonstrated a YS of 32.9 MPa, UTS of 84.5 MPa and % elongation of 28.6%. These values are consistent with published behavior of AA1100 alloys with an F-temper [102]. The addition of GNPs had a measurable effect on the mechanical properties of the Al matrix. The tensile strength increased marginally, with the 0.25 wt.% GNP concentration showing the greatest improvement. This concentration exhibited a 0.2% YS of 42.9 MPa, and UTS of 89.7 MPa, which was an improvement of 0.2% offset YS and UTS by 30.3% and 6.1%, respectively, compared to the control sample. The nano-alloy with 0.50 wt.% GNP showed a 28.6% improvement in the 0.2% YS with 42.3 MPa and a 3.0% improvement in UTS with 87.1 MPa. Similarly, the nano-alloy with 1 wt.% GNP showed a 21.3% increase in 0.2% YS with 39.9 MPa, and a 0.6% decrease in UTS, with 84.0 MPa.

Similar improvements in UTS and YS were observed by other researchers incorporating graphene into Al matrix. Notably Rashad *et al.* [51] evaluated the YS and UTS of Al/GNP composites synthesized using pure Al powder and GNP powder by a solution based powder metallurgy method. The GNP content was varied at 0.25 wt.%, 0.50 wt.% and 1 wt.%. With the addition of GNP additives, the as-extruded samples recorded an improvement in both YS and UTS values with the increase in GNP content. At a GNP content of 1 wt.%, a maximum increase of 29.4% in YS and 9.1% in UTS were observed, compared to the control sample's YS of 112 MPa and UTS of 186 MPa. Wang *et al.* [46] also reported a 62% increase in the UTS of Al composites reinforced with 0.3 wt.% rGO nanosheets. Shin *et al.* varied the vol.% of FLG in to evaluate the mechanical properties of ball milled/hot rolled Al/FLG composites. A trend of improving YS and UTS values with increasing FLG content was observed, with a maximum increase of 71.8% in YS, and a maximum increase of

57.9% in UTS at 0.7 vol.% FLG, compared to the control sample values of 262 MPa and 285 MPa for YS and UTS respectively.

Strengthening in metals at room temperature occurs by impedance to dislocation motion from grain boundaries, second phases, and strain hardening (increased dislocation density). Strengthening may also be dependent on the effectiveness of the interfacial bonding formed during alloy synthesis [11], [86], [104]. Along with this phenomenon, Wang *et al.* [46] discussed the effect of dislocation strengthening in the Al/graphene composite samples. A mismatch between the thermal expansion coefficients of the metal matrix and the additive can cause the plastic deformation along the metal/reinforcement interface during cooling from an elevated temperature. Low yield stresses of the metal matrix at high processing temperatures of 500 °C produced residual thermal stresses during cooling. Localized dislocations at the interfaces are hence formed, which contribute to the improvement in yield strength of the composites [105], [106].

Increases in the yield stress of Al/graphene composites have also been attributed to grain boundary strengthening [7]. The graphene homogenously dispersed in the Al matrix have been hypothesized to act as sites for grain boundary pinning, thus preventing grains from growing into coarser profiles during recrystallization [36]. This phenomenon adds additional resistance for the dislocations to propagate in the metal microstructure. Increases in yield strength are predicted with the Hall-Petch relationship, given in Equation (15):

$$\sigma_y = \sigma_o + \frac{k_y}{\sqrt{d}} \qquad \text{Equation (15)}$$

where σ_y the YS of the material, σ_o is the friction stress during dislocation slip, k_y is a material constant, and d is the grain size of Al. As shown, the yield strength of the metal increases with the decrease in grain size, which has been discussed to occur due to the presence of graphene in the Al matrix. The analysis of the mechanical properties of Al reinforced with multiwalled carbon nanotubes by Choi *et al.* [107] showed that the decrease in grain size from 200 nm to 72 nm with the inclusion of the carbon nanotubes resulted in an increase of yield stress of the composite from 238 MPa to 283 MPa.

The increases in UTS and YS can therefore be attributed to some combination of the aforementioned strengthening mechanisms. The presence of graphene flakes exfoliated from the GNPs in the nano-alloy microstructure adds new heterogenous interfaces which lead to 'pinning' the dislocations to reduce pathways for dislocation motion [108]. On the other hand, the decrease in YS and UTS in the 0.50 wt.% and 1 wt.% Al/GNP samples can be attributed to agglomeration of the exfoliated graphene additives as well as poorer interfacial contact between the Al matrix and GNP. The resultant ineffective load transfer due to reduced interfacial surface area in these nano-alloys may decrease the improvement in mechanical performance brought about by the increase in dislocations at the interface [109]. Improved electrical conductivity of the AA1100 matrix with the addition of GNPs observed in this study indicates that the second phase graphene may be present along the Al grain boundaries rather than inside the grains.

The elongation of the Al/GNP samples decreased with increasing GNP content in the nano-alloy wires. The control sample showed an elongation 28.6%. The 0.25 wt.%, 0.50 wt.% and 1 wt.% Al/GNP samples showed elongations of 26.2%, 22.2% and 16.6% respectively, which translated to respective decreases of 8.2%, 22.4%, and 41.9% compared to the control sample. The decrease in elongation is consistent with the behavior of Al/graphene composites seen in literature. Rashad *et al.* [51] reported a decrease in % elongation with the increase in graphene content, with the 0.50 wt.%

and 1 wt.% samples showing a decrease of 27.8% and 44.4% respectively, compared to the 18.0% elongation of the control sample. The fractured samples were observed to have numerous cavities and voids on the fracture surface, along with a sharp decrease in the size of the dimples on the fracture surfaces. The authors attributed the decrease in elongation to the domination of van der Waals interactions in the agglomerated graphene over the mechanical bonding at the Al/graphene interfaces under loading conditions. Brittle fracture was attributed to cleavage at the Al/graphene interfaces, rather than the plastic failure in the dimpled networks of the Al substrate at the fracture point [110]. Similar decreasing trends in elongation were also reported by Shin *et al.* [11]. Their 0.7 vol.% Al/graphene composites recorded the highest YS and UTS while the elongation decreased by almost 77%, from 13% to 3%. This phenomenon was attributed to the increased surface area of the graphene, leading to restricted plastic flow in the Al matrix between the embedded graphene flakes. This facilitates an earlier initiation of void nucleation and consequent brittle fracture at the Al/graphene interface [104]. Bisht *et al.* [86] also saw decreasing ductility when the graphene nanoplatelets content in Al/graphene nano-platelets composites was varied from 0 wt.% to 5 wt.%. The 5 wt.% Al/ graphene nano-platelets composite sample in the authors' study recorded the largest decrease of 90.4%, compared to an elongation of 2.6% in the control sample. These observations are consistent with this thesis' results, as observed in Figure 11. The 1 wt.% Al/GNP nano-alloy, also showed the largest decrease in elongation compared to the control sample, indicating ductility consistently decreased with increase in GNP content

5.3 Al/GNP nano-alloy wire dimensions

The flow stress characteristics of the Al/GNP nano-alloys were reflected in the extrusion force data recorded during the extrusion of the wire samples. The extrusion pressure P_e is the total work performed, which is the ideal work required for deformation W_i divided by the extrusion efficiency η. This can be expressed as a function of the flow stress, σ_f, extrusion ratio, r, and efficiency, η. [111], as shown in Equation (16).

$$P_e = \frac{W_i}{\eta} = \frac{\sigma_f \ln r}{\eta} \qquad \text{Equation (16)}$$

Figure 12 shows the ram pressure applied during the four extrusion trials of the Al/GNP nano-alloys with 0 – 1 wt.% GNPs at a constant ram speed of 0.05 mm/s. The increase in GNP content in the Al/GNP billets correlates to an increase in extrusion pressure which is attributed to an increase in flow stress.

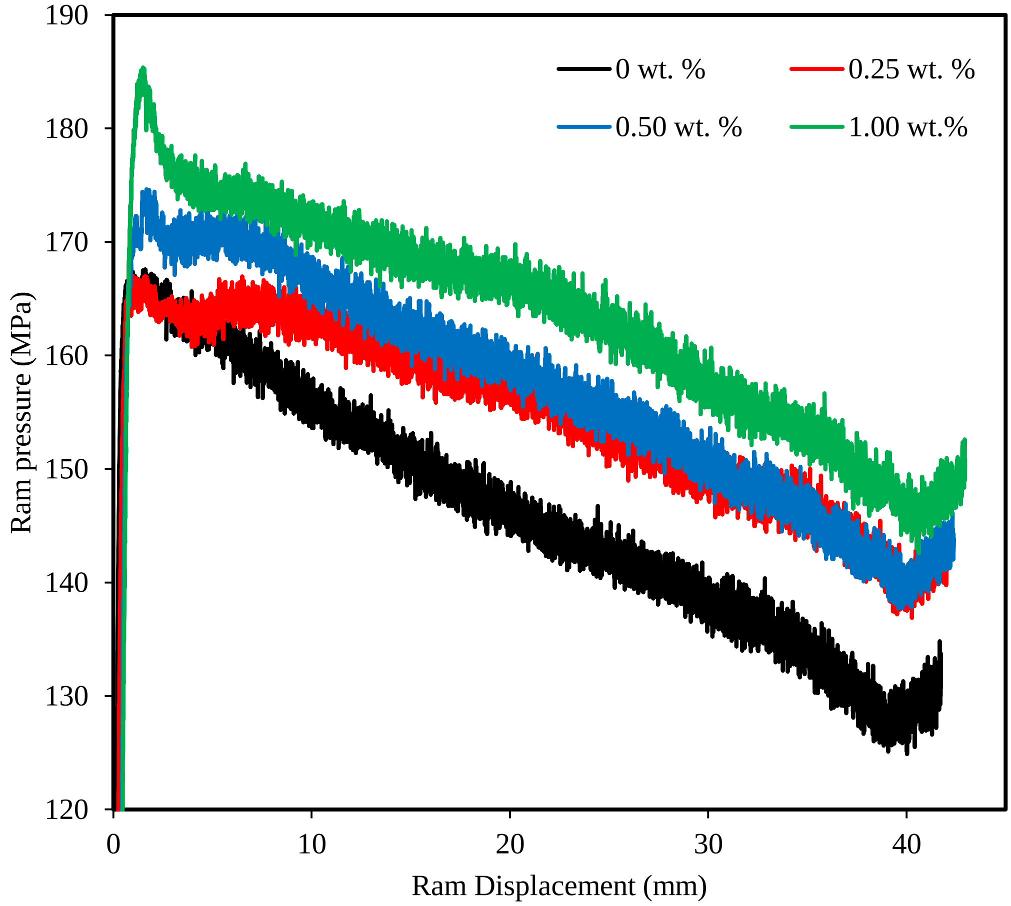

Figure 12. Extrusion pressures of Al/GNP nano-alloy wires at ram speed of 0.05 mm/s.

The ram pressure data also show an increase towards the end of the stroke. This suggests a change in the metal flow field in the deformation zone as the ram approaches the end of the extrusion cycle [112].

The extrusion data was consistent with existing data of direct extrusion of metals [112]. Figure 13 shows a schematic of the 2 regions under the extrusion data curve which can be identified.

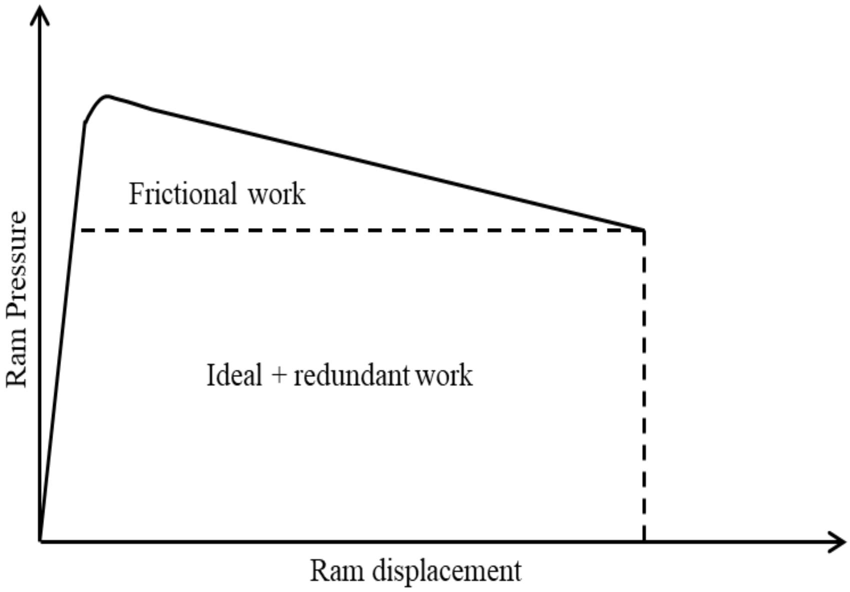

Figure 13. Representative plot of typical ram pressure/displacement profile of Al.

The lower region is a combination of ideal deformation and redundant (non-uniform) deformation work. These components are solely dependent on the Al material properties, and the extrusion parameters [111].

The upper region is the work performed by the ram to overcome friction between the container and the billet. This is dependent on the billet length, as the frictional force decreases with ram displacement, since the surface area of the billet in contact with the container decreases as the extrusion progresses.

The consolidated Al/GNP billets had lengths in the range of 54.5 – 62.3 mm prior to extrusion. The extruded wires had an average diameter of 2.03 mm (corresponding to 12 AWG), and a length of 2.75 – 2.86 m. Table 8 shows the individual dimensions of the extruded Al/GNP nano-alloy wire samples.

Table 8. Diameter and usable lengths of extruded Al/GNP nano-alloy wires.

GNP content (wt.%)	Average diameter (mm)	Length (m)
0.00 (Control)	2.036 ± 0.0015	2.76
0.25	2.012 ± 0.0747	2.78
0.50	2.032 ± 0.0025	2.80
1.00	2.031 ± 0.0042	2.94

CHAPTER 6: CONCLUSIONS

An improvement in electrical performance was achieved in AA1100 aluminum by special alloying with graphite nano-particle flakes and a unique hot extrusion process. Aluminum/nano-graphite alloys, with graphite nanoparticles contents of 0, 0.25, 0.50 and 1 wt.% were synthesized using a unique approach that involved the consolidation of graphite nanoparticle-coated AA1100 profiles, followed by cold pressing and hot-extrusion to obtain 2.0 mm diameter wires. The electrical and mechanical properties were an improvement over control samples made of AA1100 profiles processed under the same conditions. Electrical conductivity and current density were determined at 20 °C, 60 °C and 90 °C. Room temperature mechanical properties included the 0.2% yield strength, the ultimate tensile strength, and total elongation.

The best overall electrical performance was achieved with a nano-graphite concentration of 0.25 wt. %. At room temperature, this wire's electrical conductivity and current density increased by 2% and 8%, respectively. At 90°C, electrical conductivity and current density were 6.9% and 14.8% higher than the control sample, respectively. At 90 °C, the alloy with 1 wt.% nano-graphite showed the highest electrical conductivity improvement which was 8.5%. The results suggest that the shear stresses in the deformation zone (during hot extrusion) were sufficient to cause the exfoliation of graphite nanoparticles into highly conductive graphene-like entities. The shear stress in the deformation zone was estimated using the Zener-Hollomon model for AA1100 alloy and compared with the reported values to delaminate graphite into monolayer/few-layer graphene.

The mechanical properties also demonstrated similar trends, with the 0.25 wt.% samples achieving the highest increase in yield strength and ultimate tensile strength, at 30% and 6%, respectively. The ductility of the nano-alloy wire samples decreased with increasing graphite nanoparticle content, and this is consistent behavior for second-phase alloying. The improvements in room temperature and elevated temperature electrical properties also indicate minimal of aluminum carbide formation during hot extrusion. This, along with the improvement of mechanical properties, demonstrates the effectiveness of using graphite nano-particles to augment the bulk electrical conductivity of commercially used aluminum alloys.

Future work will be to extensively characterize the microstructure of the nano-alloys using conventional light and electron microscopy with energy dispersive x-ray spectroscopy. Using the data presented herein, model development of the electrical properties of aluminum/nano-graphite alloys would enhance understanding of electron scattering and phonon transport mechanisms. Finally, it will be important to characterize the aluminum-graphene interface using Raman spectroscopy to determine its nature as a function of the manufacturing process parameters.

REFERENCES

[1] J. R. Davis, *Aluminum and Aluminum Alloys*. 2001.

[2] G. E. Totten and D. S. MacKenzie, *Handbook of Aluminum: Vol. 1: Physical Metallurgy and Processes*, vol. 1. CRC Press, 2003.

[3] J. R. Davis, *Corrosion of aluminum and aluminum alloys*. Asm International, 1999.

[4] R. Brandt and G. Neuer, "Electrical resistivity and thermal conductivity of pure aluminum and aluminum alloys up to and above the melting temperature," *Int. J. Thermophys.*, vol. 28, no. 5, pp. 1429–1446, 2007.

[5] J. Hatch, *Aluminum: properties and physical metallurgy*. ASM International, 1984.

[6] C. Hunter, "Aluminum Building Wire Installation and Terminations," *Iaei News*, no. February, p. 78–85. Disponible:, 2006.

[7] S. C. Tjong, "Recent progress in the development and properties of novel metal matrix nanocomposites reinforced with carbon nanotubes and graphene nanosheets," *Mater. Sci. Eng. R Reports*, vol. 74, no. 10, pp. 281–350, Oct. 2013.

[8] H. Kwon, M. Estili, K. Takagi, T. Miyazaki, and A. Kawasaki, "Combination of hot extrusion and spark plasma sintering for producing carbon nanotube reinforced aluminum matrix composites," *Carbon N. Y.*, vol. 47, pp. 570–577, 2009.

[9] S. F. Bartolucci, J. Paras, M. A. Rafiee, J. Rafiee, S. Lee, D. Kapoor, and N. Koratkar, "Graphene-aluminum nanocomposites," *Mater. Sci. Eng. A*, vol. 528, no. 27, pp. 7933–7937, 2011.

[10] H. Kwon, D. H. Park, J. F. Silvain, and A. Kawasaki, "Investigation of carbon

nanotube reinforced aluminum matrix composite materials," *Compos. Sci. Technol.*, vol. 70, no. 3, pp. 546–550, Mar. 2010.

[11] S. E. Shin, H. J. Choi, J. H. Shin, and D. H. Bae, "Strengthening behavior of few-layered graphene/aluminum composites," *Carbon N. Y.*, vol. 82, no. C, pp. 143–151, 2015.

[12] F. Ogawa and C. Masuda, "Fabrication of carbon nanofiber-reinforced aluminum matrix composites assisted by aluminum coating formed on nanofiber surface by in situ chemical vapor deposition," *Mater. Res. Express*, vol. 2, no. 1, p. 15601, 2015.

[13] S. E. Shin, Y. J. Ko, and D. H. Bae, "Mechanical and thermal properties of nanocarbon-reinforced aluminum matrix composites at elevated temperatures," 2016.

[14] K. S. Reddy, D. Sreedhar, K. D. Kumar, and G. P. Kumar, "Role of Reduced Graphene Oxide on Mechanical-thermal Properties of Aluminum Metal Matrix Nano Composites," *Mater. Today Proc.*, vol. 2, no. 4–5, pp. 1270–1275, 2015.

[15] R. H. R. Castro, P. Hidalgo, and E. C. Diniz, "Enhanced electrical conduction in aluminum wires coated with carbon nanotubes," *Mater. Lett.*, vol. 65, no. 2, pp. 271–274, Jan. 2011.

[16] C. L. Xu, B. Q. Wei, R. Z. Ma, J. Liang, X. K. Ma, and D. H. Wu, "Fabrication of aluminum–carbon nanotube composites and their electrical properties," *Carbon N. Y.*, vol. 37, pp. 855–858, 1999.

[17] D. Forrest, I. Jasiuk, L. Brown, and P. Joyce, "Novel Metal-Matrix Composites with Integrally-Bound Nanoscale Carbon," *Nanotechnol. 2012 Adv. Mater. CNTs, Part. Film. Compos.*, vol. 1, 2012.

[18] S. Iijima and K. Tanaka, "Carbon Nanotubes and Graphene (Second Edition),"

Second Edi., K. Tanaka and S. Iijima, Eds. Oxford: Elsevier, 2014, p. iii-.

[19] A. K. Geim and K. S. Novoselov, “The rise of graphene,” *Nat. Mater.*, vol. 6, no. 3, pp. 183–191, Mar. 2007.

[20] M. J. Allen, V. C. Tung, and R. B. Kaner, “Honeycomb Carbon: A Review of Graphene,” *Chem. Rev.*, vol. 110, no. 1, pp. 132–145, Jan. 2010.

[21] K. S. Novoselov, A. K. Geim, S. V. Morozov, D. Jiang, Y. Zhang, S. V. Dubonos, I. V. Grigorieva, and A. A. Firsov, “Electric Field Effect in Atomically Thin Carbon Films,” *Science (80-.).*, vol. 306, pp. 666–669, 2004.

[22] Y. Zhu, S. Murali, W. Cai, X. Li, J. W. Suk, J. R. Potts, and R. S. Ruoff, “Graphene and graphene oxide: Synthesis, properties, and applications,” *Adv. Mater.*, vol. 22, no. 35, pp. 3906–3924, 2010.

[23] H.-Q. Wu, C.-Y. Linghu, H.-M. Lu, and H. Qian, “Graphene applications in electronic and optoelectronic devices and circuits,” *Chinese Phys. B*, vol. 22, no. 9, p. 098106, 2013.

[24] J. S. Bunch, A. M. van der Zande, S. S. Verbridge, I. W. Frank, D. M. Tanenbaum, J. M. Parpia, H. G. Craighead, and P. L. McEuen, “Electromechanical resonators from graphene sheets,” *Science (80-.).*, vol. 315, no. 5811, pp. 490–493, 2007.

[25] S. Ghosh, W. Bao, D. L. Nika, S. Subrina, E. P. Pokatilov, C. N. Lau, and A. a Balandin, “Dimensional crossover of thermal transport in few-layer graphene.,” *Nat. Mater.*, vol. 9, no. 7, pp. 555–558, 2010.

[26] C. Riedl, “Epitaxial Graphene on Silicon Carbide Surfaces: Growth, Characterization, Doping and Hydrogen Intercalation,” 2010.

[27] X. Du, I. Skachko, A. Barker, and E. Y. Andrei, “Approaching ballistic transport in suspended graphene,” *Nat. Nanotechnol.*, vol. 3, no. 8, pp. 491–

495, Aug. 2008.

[28] C. Lee, X. Wei, J. W. Kysar, and J. Hone, “Measurement of the elastic properties and intrinsic strength of monolayer graphene.,” *Sci. Mag.*, vol. 321, no. 5887, pp. 385–388, 2008.

[29] A. A. Balandin, S. Ghosh, W. Bao, I. Calizo, D. Teweldebrhan, F. Miao, and C. N. Lau, “Superior Thermal Conductivity of Single-Layer Graphene,” *Nano Lett.*, vol. 8, no. 3, pp. 902–907, 2008.

[30] R. R. Nair, P. Blake, a. N. Grigorenko, K. S. Novoselov, T. J. Booth, T. Stauber, N. M. R. Peres, and a. K. Geim, “Fine Structure Constant Defines Visual Transperency of Graphene,” *Science (80-.).*, vol. 320, no. June, p. 2008, 2008.

[31] A. K. Geim, “Graphene: Status and Prospects,” *Prospects*, vol. 324, no. 5934, pp. 1–8, 2009.

[32] C. Soldano, S. Talapatra, and S. Kar, *Carbon Nanotubes and Graphene Nanoribbons: Potentials for Nanoscale Electrical Interconnects*, vol. 2, no. 3. 2013.

[33] A. Bezryadin, A. R. M. Verschueren, S. J. Tans, and C. Dekker, “Multiprobe Transport Experiments on Individual Single-Wall Carbon Nanotubes,” *Phys. Rev. Lett.*, vol. 80, no. 18, pp. 4036–4039, 1998.

[34] M. Paradise and T. Goswami, “Carbon nanotubes - Production and industrial applications,” *Mater. Des.*, vol. 28, no. 5, pp. 1477–1489, 2007.

[35] H. Dai, “Carbon nanotubes: Synthesis, integration, and properties,” *Acc. Chem. Res.*, vol. 35, no. 12, pp. 1035–1044, 2002.

[36] A. Nieto, A. Bisht, D. Lahiri, C. Zhang, and A. Agarwal, “Graphene reinforced metal and ceramic matrix composites: a review,” *Int. Mater. Rev.*, vol. 62, no.

5, pp. 241–302, 2017.

[37] L. Yan, Z. Tan, G. Ji, Z. Li, G. Fan, D. Schryvers, A. Shan, and D. Zhang, "A quantitative method to characterize the Al4C3 -formed interfacial reaction: The case study of MWCNT/Al composites," *Mater. Charact.*, vol. 112, pp. 213–218, 2016.

[38] D. Poirier, R. Gauvin, and R. A. L. Drew, "Structural characterization of a mechanically milled carbon nanotube/aluminum mixture," *Compos. Part A*, vol. 40, pp. 1482–1489, 2009.

[39] Q. Liu, L. Ke, F. Liu, C. Huang, and L. Xing, "Microstructure and mechanical property of multi-walled carbon nanotubes reinforced aluminum matrix composites fabricated by friction stir processing," *Mater. Des.*, vol. 45, pp. 343–348, 2013.

[40] M. Lee, Y. Choi, K. Sugio, K. Matsugi, and G. Sasaki, "Effect of aluminum carbide on thermal conductivity of the unidirectional CF/Al composites fabricated by low pressure infiltration process," *Compos. Sci. Technol.*, vol. 97, pp. 1–5, 2014.

[41] L. Yan, Z. Tan, G. Ji, Z. Li, G. Fan, D. Schryvers, A. Shan, and D. Zhang, "A quantitative method to characterize the Al4C3-formed interfacial reaction: The case study of MWCNT/Al composites," *Mater. Charact.*, vol. 112, pp. 213–218, 2016.

[42] Q. Li, C. A. Rottmair, and R. F. Singer, "CNT reinforced light metal composites produced by melt stirring and by high pressure die casting," *Compos. Sci. Technol.*, vol. 70, no. 16, pp. 2242–2247, 2010.

[43] T. Laha, S. Kuchibhatla, S. Seal, W. Li, and A. Agarwal, "Interfacial phenomena in thermally sprayed multiwalled carbon nanotube reinforced

aluminum nanocomposite," *Acta Mater.*, vol. 55, no. 3, pp. 1059–1066, 2007.

[44] A. Nittala, K. Kappagantula, J. Smith, and F. Kraft, "Effect of carbon nanostructures on aluminum metal matrix composites performance," in *Materials Science & Technology*, 2017.

[45] M. Rashad, F. Pan, A. Tang, and M. Asif, "Effect of Graphene Nanoplatelets addition on mechanical properties of pure aluminum using a semi-powder method," *Prog. Nat. Sci. Mater. Int.*, vol. 24, no. 2, pp. 101–108, 2014.

[46] J. Wang, Z. Li, G. Fan, H. Pan, Z. Chen, and D. Zhang, "Reinforcement with graphene nanosheets in aluminum matrix composites," *Scr. Mater.*, vol. 66, no. 8, pp. 594–597, Apr. 2012.

[47] W. Tian, S. Li, B. Wang, X. Chen, J. Liu, and M. Yu, "Graphene-reinforced aluminum matrix composites prepared by spark plasma sintering," *Int. J. Miner. Metall. Mater.*, vol. 23, no. 6, pp. 723–729, 2016.

[48] A. F. Boostani, S. Yazdani, R. T. Mousavian, S. Tahamtan, R. Azari Khosroshahi, D. Wei, D. Brabazon, J. Z. Z. Xu, X. M. M. Zhang, Z. Y. Y. Jiang, A. Fadavi Boostani, S. Yazdani, R. Taherzadeh Mousavian, S. Tahamtan, R. Azari Khosroshahi, D. Wei, D. Brabazon, J. Z. Z. Xu, X. M. M. Zhang, and Z. Y. Y. Jiang, "Strengthening mechanisms of graphene sheets in aluminium matrix nanocomposites," *Mater. Des.*, vol. 88, pp. 983–989, 2015.

[49] L. A. Yolshina, R. V. Muradymov, I. V. Korsun, G. A. Yakovlev, and S. V. Smirnov, "Novel aluminum-graphene and aluminum-graphite metallic composite materials: Synthesis and properties," *J. Alloys Compd.*, vol. 663, pp. 449–459, 2016.

[50] R. Pérez-Bustamante, D. Bolaños-Morales, J. Bonilla-Martínez, I. Estrada-Guel, and R. Martínez-Sánchez, "Microstructural and hardness behavior of

graphene-nanoplatelets/aluminum composites synthesized by mechanical alloying," *J. Alloys Compd.*, vol. 615, no. S1, pp. S578–S582, 2015.

[51] M. Rashad, F. Pan, Z. Yu, M. Asif, H. Lin, and R. Pan, "Investigation on microstructural, mechanical and electrochemical properties of aluminum composites reinforced with graphene nanoplatelets," *Prog. Nat. Sci. Mater. Int.*, vol. 25, no. 5, pp. 460–470, 2015.

[52] S. J. Yan, S. L. Dai, X. Y. Zhang, C. Yang, Q. H. Hong, J. Z. Chen, and Z. M. Lin, "Investigating aluminum alloy reinforced by graphene nanoflakes," 2014.

[53] V. Jain, A. Kumar, and A. Dhar, "Microscopic and spectroscopic evaluation of SPS sintered aluminium-graphene (Al-Gr) nanocomposites," *Adv. Mater. Proc.*, vol. 2, no. 3, pp. 146–151, 2017.

[54] J. L. Li, Y. C. Xiong, X. D. Wang, S. J. Yan, C. Yang, W. W. He, J. Z. Chen, S. Q. Wang, X. Y. Zhang, and S. L. Dai, "Microstructure and tensile properties of bulk nanostructured aluminum/graphene composites prepared via cryomilling," *Mater. Sci. Eng. A*, vol. 626, pp. 400–405, 2015.

[55] L. Brown, P. Joyce, D. Forrest, and J. Wolk, "Physical and Mechanical Characterization of a Nanocarbon Infused Aluminum-Matrix Composite," *Mater. Perform. Charact.*, vol. 3, no. 1, pp. 2014–2015, 2014.

[56] F. A. Chyada, A. R. Jabur, and H. A. Alwan, "Effect addition of graphene on electrical conductivity and tensile strength for Recycled electric power transmission wires," *Energy Procedia*, vol. 119, pp. 121–130, Jul. 2017.

[57] B. F. Schultz, J. B. Ferguson, and P. K. Rohatgi, "Microstructure and hardness of Al2O3 nanoparticle reinforced Al–Mg composites fabricated by reactive wetting and stir mixing," *Mater. Sci. Eng. A*, vol. 530, pp. 87–97, 2011.

[58] A. J. Cook and P. S. Werner, "Pressure infiltration casting of metal matrix

composites," *Mater. Sci. Eng. A*, vol. 144, no. 1–2, pp. 189–206, Oct. 1991.

[59] M. K. Surappa, "Microstructure evolution during solidification of DRMMCs (Discontinuously reinforced metal matrix composites): State of art," *J. Mater. Process. Technol.*, vol. 63, no. 1–3, pp. 325–333, Jan. 1997.

[60] J.-Y. Lim, S.-I. Oh, Y.-C. Kim, K.-K. Jee, Y.-M. Sung, and J. H. Han, "Effects of CNF dispersion on mechanical properties of CNF reinforced A7xxx nanocomposites," *Mater. Sci. Eng. A*, vol. 556, pp. 337–342, Oct. 2012.

[61] Z. G. Liu, X. B. Mang, L. H. Chai, and Y. Y. Chen, "Interface study of carbon fibre reinforced Al–Cu composites," *J. Alloys Compd.*, vol. 504, pp. S512–S514, Aug. 2010.

[62] S. . Ip, R. Sridhar, J. . Toguri, T. . Stephenson, and A. E. . Warner, "Wettability of nickel coated graphite by aluminum," *Mater. Sci. Eng. A*, vol. 244, no. 1, pp. 31–38, Mar. 1998.

[63] K. P. So, J. C. Jeong, J. G. Park, H. K. Park, Y. H. Choi, D. H. Noh, D. H. Keum, H. Y. Jeong, C. Biswas, C. H. Hong, and Y. H. Lee, "SiC formation on carbon nanotube surface for improving wettability with aluminum," *Compos. Sci. Technol.*, vol. 74, pp. 6–13, Jan. 2013.

[64] C.-H. Jeon, Y.-H. Jeong, J.-J. Seo, H. N. Tien, S.-T. Hong, Y.-J. Yum, S.-H. Hur, and K.-J. Lee, "Material properties of graphene/aluminum metal matrix composites fabricated by friction stir processing," *Int. J. Precis. Eng. Manuf.*, vol. 15, no. 6, pp. 1235–1239, 2014.

[65] F. H. Latief and E. S. M. Sherif, "Effects of sintering temperature and graphite addition on the mechanical properties of aluminum," *J. Ind. Eng. Chem.*, vol. 18, no. 6, pp. 2129–2134, 2012.

[66] G. Xie, O. Ohashi, T. Yoshioka, M. Song, K. Mitsuishi, H. Yasuda, K. Furuya,

and T. Noda, “Effect of Interface Behavior between Particles on Properties of Pure Al Powder Compacts by Spark Plasma Sintering.,” *Materials Transactions*, vol. 42, no. 9. pp. 1846–1849, 2001.

[67] W. Zhou, S. Bang, H. Kurita, T. Miyazaki, Y. Fan, and A. Kawasaki, “Interface and interfacial reactions in multi-walled carbon nanotube-reinforced aluminum matrix composites,” *Carbon N. Y.*, vol. 96, pp. 919–928, 2016.

[68] W. Zhou, T. Yamaguchi, K. Kikuchi, N. Nomura, and A. Kawasaki, “Effectively enhanced load transfer by interfacial reactions in multi-walled carbon nanotube reinforced Al matrix composites,” *Acta Mater.*, vol. 125, pp. 369–376, Feb. 2017.

[69] A. Zameshin, M. Popov, V. Medvedev, S. Perfilov, R. Lomakin, S. Buga, V. Denisov, A. Kirichenko, E. Skryleva, E. Tatyanin, V. Aksenenkov, and V. Blank, “Electrical conductivity of nanostructured and C60-modified aluminum,” *Appl. Phys. A Mater. Sci. Process.*, vol. 107, no. 4, pp. 863–869, Jun. 2012.

[70] J. Tokutomi, T. Uemura, S. Sugiyama, J. Shiomi, and J. Yanagimoto, “Hot extrusion to manufacture the metal matrix composite of carbon nanotube and aluminum with excellent electrical conductivities and mechanical properties,” *CIRP Ann. - Manuf. Technol.*, vol. 64, no. 1, pp. 257–260, 2015.

[71] F. Gao, J. Qu, and M. Yao, “Electrical resistance at carbon nanotube/copper interfaces: Capped versus open-end carbon nanotubes,” *Mater. Lett.*, vol. 82, pp. 184–187, 2012.

[72] Y. Tang, H. Cong, R. Zhong, and H.-M. Cheng, “Thermal expansion of a composite of single-walled carbon nanotubes and nanocrystalline aluminum,” *Carbon N. Y.*, vol. 42, no. 15, pp. 3260–3262, Jan. 2004.

[73] F. H. Latief, E. S. M. Sherif, A. A. Almajid, and H. Junaedi, “Fabrication of exfoliated graphite nanoplatelets-reinforced aluminum composites and evaluating their mechanical properties and corrosion behavior,” *J. Anal. Appl. Pyrolysis*, vol. 92, no. 2, pp. 485–492, 2011.

[74] S. Zhou, X. Zhang, Z. Ding, C. Min, G. Xu, and W. Zhu, “Fabrication and tribological properties of carbon nanotubes reinforced Al composites prepared by pressureless infiltration technique,” *Compos. Part A Appl. Sci. Manuf.*, vol. 38, no. 2, pp. 301–306, Feb. 2007.

[75] S. R. Bakshi, A. K. Keshri, and A. Agarwal, “A comparison of mechanical and wear properties of plasma sprayed carbon nanotube reinforced aluminum composites at nano and macro scale,” *Mater. Sci. Eng. A*, vol. 528, no. 9, pp. 3375–3384, Apr. 2011.

[76] ASTM International, “ASTM B221-14, Standard Specification for Aluminum and Aluminum-Alloy Extruded Bars, Rods, Wire, Profiles, and Tubes.” 2014.

[77] F. F. Kraft and J. Kochis, “Hot Extrusion of Thin-Wall Multichannel Copper Profiles,” *J. Manuf. Sci. Eng.*, vol. 135, no. 6, Nov. 2013.

[78] ASTM International, “ASTM B193-16 Standard Test Method for Resistivity of Electrical Conductor Materials,” www.astm.org, West Conshohocken, PA, 2016.

[79] “ASTM B557 - 15 Standard Test Methods for Tension Testing Wrought and Cast Aluminum- and Magnesium-Alloy Products,” West Conshohocken, PA, 2015.

[80] K. Instruments, “Keithley 2260B-30-72 DC Power Supply.”

[81] K. Instruments, “Keithley Model 2182A Nanovoltmeter Data Sheet,” 2013.

[82] Keyence, “Keyence LS 7601 Data sheet,” 2017.

[83] Instron Corporation, “Instron Series 5500 Datasheet/manual,” 2005.

[84] Mitutoyo, “Long ABSOLUTE Digimtic Caliper 500 Series,” 2017. [Online]. Available: https://www.mitutoyo.co.jp/eng/useful/catalog-2016/index.html#page=229.

[85] S.-Y. Chang, C.-F. Chen, S.-J. Lin, and T. Z. Kattamis, “Electrical resistivity of metal matrix composites,” *Acta Mater.*, vol. 51, no. 20, pp. 6291–6302, Dec. 2003.

[86] A. Bisht, M. Srivastava, R. M. Kumar, I. Lahiri, and D. Lahiri, “Strengthening mechanism in graphene nanoplatelets reinforced aluminum composite fabricated through spark plasma sintering,” *Mater. Sci. Eng. A*, vol. 695, pp. 20–28, May 2017.

[87] F. C. Campbell, “Aluminum,” in *Elements of Metallurgy and Engineering Alloys*, F. C. Campbell, Ed. ASM International, 2008, pp. 487–508.

[88] R. Mahmudi, “Grain boundary strengthening in a fine grained aluminum alloy,” *Scr. Metall. Mater. States)*, vol. 32, no. 5, 1995.

[89] T. Hu, K. Ma, T. D. Topping, J. M. Schoenung, and E. J. Lavernia, “Precipitation phenomena in an ultrafine-grained Al alloy,” *Acta Mater.*, vol. 61, no. 6, pp. 2163–2178, Apr. 2013.

[90] K. Ma, H. Wen, T. Hu, T. D. Topping, D. Isheim, D. N. Seidman, E. J. Lavernia, and J. M. Schoenung, “Mechanical behavior and strengthening mechanisms in ultrafine grain precipitation-strengthened aluminum alloy,” *Acta Mater.*, vol. 62, pp. 141–155, Jan. 2014.

[91] X. Y. Fang, X. X. Yu, H. M. Zheng, H. B. Jin, L. Wang, and M. S. Cao, “Temperature- and thickness-dependent electrical conductivity of few-layer graphene and graphene nanosheets,” *Phys. Lett. Sect. A Gen. At. Solid State*

Phys., vol. 379, no. 37, pp. 2245–2251, 2015.

[92] P. Boggild, D. M. A. Mackenzie, P. Whelan, D. H. Petersen, J. C. D. Buron, A. Zurutuza, J. C. Gallop, L. Hao, and P. U. Jepsen, “Mapping the electrical properties of large-area graphene,” *2D Mater.*, 2017.

[93] T. Sheppard, “Temperature and speed effects in hot extrusion of aluminium alloys,” *Met. Technol.*, vol. 8, no. April, pp. 130–141, 1981.

[94] Y. Sun, Q. Pan, Z. Huang, W. Wang, X. Wang, M. Li, and J. Lai, “Evolutions of diffusion activation energy and Zener–Hollomon parameter of ultra-high strength Al-Zn-Mg-Cu-Zr alloy during hot compression,” *Prog. Nat. Sci. Mater. Int.*, vol. 28, no. 5, pp. 635–646, Oct. 2018.

[95] H. J. McQueen, W. A. Wong, and J. J. Jonas, “Deformation of Aluminum at High Temperatures and Strain Rates,” *Can. J. Phys.*, vol. 45, no. 2, pp. 1225–1234, Feb. 1967.

[96] S. B. Brown and K. H. Kn, “An Internal Variable Constitutive Model for Hot Working of Metals,” *Int. J. Plast.*, vol. 5, pp. 95–130, 1989.

[97] T. S. Tran, S. J. Park, S. S. Yoo, T. R. Lee, and T. Y. Kim, “High shear-induced exfoliation of graphite into high quality graphene by Taylor-Couette flow,” *RSC Adv.*, vol. 6, no. 15, pp. 12003–12008, 2016.

[98] A. Seeger, “The electronic structure of point defects in metals,” *Le J. Phys. Le Radium*, vol. 23, no. 10, pp. 616–626, 1962.

[99] F. R. Fickett, “Aluminum—1. A review of resistive mechanisms in aluminum,” *Cryogenics (Guildf).*, vol. 11, no. 5, pp. 349–367, Oct. 1971.

[100] R. A. Butera and D. H. Waldeck, “The Dependence of Resistance on Temperature for Metals, Semiconductors, and Superconductors,” *J. Chem. Educ.*, vol. 74, no. 9, p. 1090, 1997.

[101] S. Kasap, C. Koughia, and H. E. Ruda, “Electrical Conduction in Metals and Semiconductors,” in *Springer Handbook of Electronic and Photonic Materials*, Cham: Springer International Publishing, 2017, pp. 1–1.

[102] J. G. Kaufman, *Properties of aluminum alloys: tensile, creep, and fatigue data at high and low temperatures*. ASM international, 1999.

[103] Z. Zhang and D. L. Chen, “Consideration of Orowan strengthening effect in particulate-reinforced metal matrix nanocomposites: A model for predicting their yield strength,” *Scr. Mater.*, vol. 54, no. 7, pp. 1321–1326, Apr. 2006.

[104] N. Chawla and Y.-L. Y. Shen, “Mechanical behavior of particle reinforced metal matrix composites,” *Adv. Eng. Mater.*, vol. 3, no. 6, pp. 357–370, 2001.

[105] R. U. Vaidya and K. . Chawla, “Thermal expansion of metal-matrix composites,” *Compos. Sci. Technol.*, vol. 50, no. 1, pp. 13–22, Jan. 1994.

[106] K. K. Chawla, “Metal Matrix Composites,” *Materials Science and Technology*. 15-Sep-2006.

[107] H. J. Choi, J. H. Shin, and D. H. Bae, “Grain size effect on the strengthening behavior of aluminum-based composites containing multi-walled carbon nanotubes,” *Compos. Sci. Technol.*, vol. 71, no. 15, pp. 1699–1705, Oct. 2011.

[108] L. Zhao, H. Lu, and Z. Gao, “Microstructure and Mechanical Properties of Al/Graphene Composite Produced by High-Pressure Torsion,” *Adv. Eng. Mater.*, vol. 17, no. 7, pp. 976–981, 2015.

[109] Z. W. Zhang, Z. Y. Liu, B. L. Xiao, D. R. Ni, and Z. Y. Ma, “High efficiency dispersal and strengthening of graphene reinforced aluminum alloy composites fabricated by powder metallurgy combined with friction stir processing,” *Carbon N. Y.*, vol. 135, pp. 215–223, Aug. 2018.

[110] D. L. McDanels, “Analysis of stress-strain, fracture, and ductility behavior of

aluminum matrix composites containing discontinuous silicon carbide reinforcement,” *Metall. Trans. A*, vol. 16, no. 6, pp. 1105–1115, Jun. 1985.

[111] F. H. William, M. C. Robert, W. F. Hosford, and R. M. Caddell, “Metal forming: Mechanics and metallurgy,” *Prentice Hall, Englewood Cliffs NJ*, vol. 7632, no. 1, pp. 250–260, 1983.

[112] V. S. Dongare, “Hot Extrusion of Carbon Nanotube - Magnesium Matrix Composite Wire.” 2014.